

Electron Beam Ion Sources

Giinter Zschornack^a, Mike Schmidt^b, Alexandra Thorn^b

a) University of Technology Dresden, Helmholtz-Zentrum Dresden-Rossendorf

and Dreebit GmbH Dresden, Germany

b) Dreebit GmbH Dresden, Germany

Abstract

Electron Beam Ion Sources (EBIS) are ion sources which work based on the principle of electron impact ionization allowing the production of very highly charged ions. The produced ions can be extracted as a DC ion beam as well as ion pulses of different time structures. In comparison to most of the other known ion sources EBIS feature ion beams with very good beam emittances and a low energy spread. Furthermore, EBIS are excellent sources of photons (X-rays, UV, EUV, visible light) from highly charged ions. This article gives an overview of EBIS physics, the principle of operation, and the known technical solutions. Using examples, the performance of EBIS as well as their applications in various fields of basic research, technology and medicine are discussed.

1 Introduction

The idea to develop Electron Beam Ion Sources (EBIS) was constituted by the need of multiply charged ions for accelerator applications to derive high final kinetic particle energies and by a general scientific interest to study exotic states of matter as represented by highly charged ions (HCIs).

Highly charged ions possess properties that differ in many ways from classical ions. Distinguishing characteristics are:

- Due to the ionization process a large amount of potential energy is stored in HCIs. For example a Xe^{44+} ion has a potential energy of about 51 keV.
- At ion-surface interactions this potential energy is released within a few 10 fs at an area of about 100 nm^2 , which leads to power densities of 10^{12} up to 10^{14} W/cm^2 .
- Due to the high power density in the surface interaction area compared to low charged ions (LCIs) HCIs produce high amounts of secondary particles such as neutrals as well as secondary electrons and secondary ions.
- HCIs possess very strong static electric fields reaching from 10^{14} V/cm up to 10^{16} V/cm .
- HCIs are characterized by a very effective stopping power (e.g. for Au^{69+} : 100 keV/nm).
- Due to their high ionic charge HCIs can be accelerated very effectively ($\propto q$ for linear accelerators and $\propto q^2$ for circular accelerators; q denotes the ion charge state).
- Nowadays, HCIs can be produced in a compact laboratory setup. Large accelerator structures are used in case of high HCI currents are necessary for a specific experiment but are not required for many applications.

These unique properties are the reason why the interest in HCIs is constantly growing and the number of applications increases. Fig. 1 gives several examples for applications of HCIs in basic research as well as technology.

Under standard conditions, HCIs are not available in the laboratory or for technological applications. They appear only in the plasma of fusion facilities, the corona of the sun, at the border of black holes, and similar exotic cosmic regions. First publications on HCIs date more than eighty years back

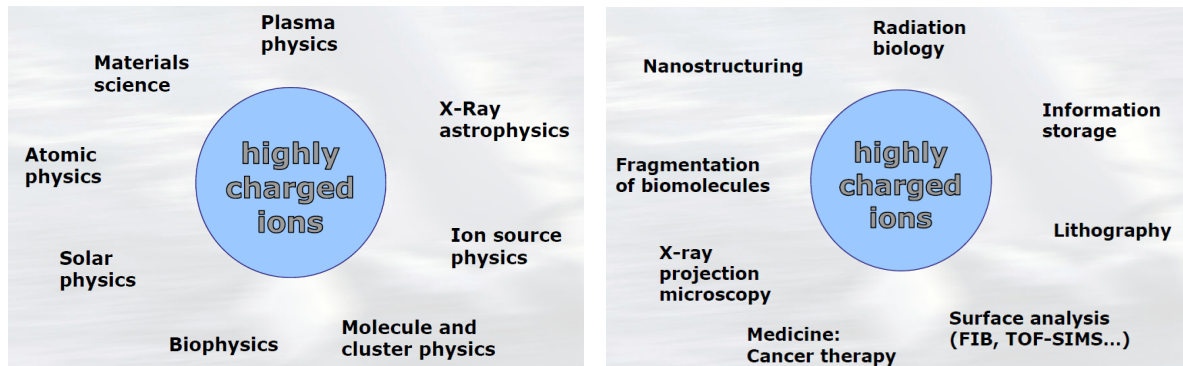


Fig. 1: Some applications of HCIs in basic research (left side) and possible applications in technology (right side).

and the number of publications has increased continuously. In first classical papers Bowen and Millikan reported on the production of Se^{20+} ions in an arc discharge [1] in 1925 and Edlen explained the origin of spectral lines in the corona of the sun as emission lines from ten- to fifteen-fold ionized iron, calcium and nickel atoms in 1942 [2].

A classical approach to produce HCIs in the laboratory is the use of ion accelerators by stripping of energetic LCI to practical all possible ion charge states. As a result of the stripping process HCIs of high kinetic energy are produced which must be decelerated in many cases for further use. Another access to HCIs is the use of powerful ion sources such as

- EBIS,
- Electron Cyclotron Resonance (ECR) ion sources (for basics see [3]) or
- laser ion sources (for basics see [4]).

This present paper is about EBIS. For details on other kinds of ion sources we refer to the citations above and the references therein. The aim of this work is to give a short up-to-date overview about the function and use of EBIS technology. More details can be found in literature, e.g. in the book of Gillaspy [5] and the paper written by Currell [39]. More detailed information about the basic physics of HCIs can be found in the review from Gillaspy [7] and the book written by Beyer and Shevelko [8].

2 EBIS: The Basic Idea

2.1 The Technical solution

EBIS/T ion sources have been known for more than 40 years and the technical design of these sources has been improved continuously with increasing technical possibilities. The principal operation scheme of an EBIS is shown in Fig. 2.

The ion production in an EBIS is based on electron impact ionization in a high-density electron beam which is compressed by a strong magnetic field produced by magnetic coils. An electron gun with a cathode of high emissivity produces the electron beam. The ions which are produced by successive electron impact ionization inside the electron beam are radially confined by the negative space charge of the electron beam and the axial confinement of the ions is achieved by superposition of electrostatic potentials generated using a minimum of three collinear drift tubes. The higher potentials on the outer drift tubes create an axial electrostatic trap. Hence, the ionization time of the ions can be controlled by switching the axial trap potentials periodically on and off.

The magnetic field for the electron beam compression is generated by a special magnet system which can consist of superconducting magnetic coils or permanent magnet rings. The electron beam is dumped in an electron beam collector where the electrons are separated from the extracted ions. Usually

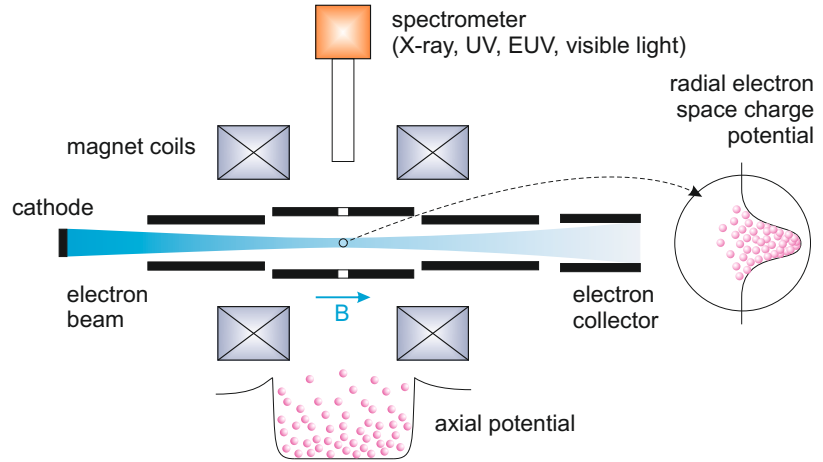


Fig. 2: Principal operation scheme of an EBIS

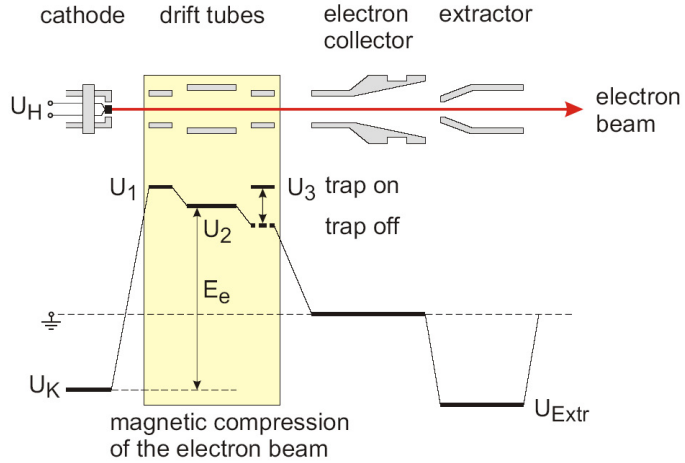


Fig. 3: Electrical scheme of EBIS operation. U_K – cathode potential, U_{Extr} – ion extraction potential, U_H – potential at the cathode heater, U_1 – trap potential at the side of the electron gun, U_3 – trap potential at the ion extraction side (switched for pulsed ion extraction), U_2 – potential at the middle drift tube

EBIS are equipped with one or more radial ports. This allows for spectrometry of electromagnetic radiation produced in the region of the ion trap during the ionization process.

The electrical scheme of EBIS operation is shown in Fig. 3 for an EBIS with three drift tubes (known are also solutions with more drift tubes). The electron energy E_e in the center of the drift tubes where the ions are produced and accumulated is

$$E_e = e (U_2 - U_K + U_e) \quad (1)$$

with U_e as the space charge potential of the electron beam which slightly decreases the final electron beam energy. The axial ion trap is controlled by switching the potential U_3 in the indicated manner. The chosen dynamics and height of the potential wall formed by the voltage U_3 allows three principal modes of source operation:

- **Permanently opened trap – transmission mode.**

The trap is permanently open and ions are produced in the electron beam without axial trapping. This mode delivers high currents of the lowest charged ions with ion beam currents up to μA .

- **Partially closed trap – leaky mode.**

Selecting a low axial potential wall a certain amount of ions with adequate kinetic energy can surpass the potential wall and is extracted continuously. This mode delivers ions with preferentially low up to intermediate ion charge states and a small fraction of higher ion charge states with ion beam currents up to nA.

- **Periodically opened and closed trap – pulsed mode.**

In this case the voltage U_3 is high enough to trap all ions axially. Periodical opening of the trap releases pulses of ions extracted with typical pulse widths in the order of some microseconds and allows to produce highest currents of HCIs (up to μA during the pulse).

Table 1 compares important practically realized parameters of cryogenic and room-temperature EBIS.

Table 1: Parameters of cryogenic and room-temperature EBIS

Parameter	cryogenic EBIS	room-temperature EBIS
magnetic system	superconducting coils (3...8) T on axis	permanent magnets (SmCo, NdFeB) (250...600) mT on axis
electron beam currents	up to A	≤ 200 mA
electron beam energies	up to 200 keV	up to 30 keV
electron beam densities	$j_e > 1000$ A/cm ²	$j_e < 500$ A/cm ²
basic vacuum	up to 10^{-12} mbar	up to 10^{-10} mbar
length of the ionization region	up to m	≤ 6 cm
ion charge states	highest ion charge states $\text{Xe}^{54+}, \text{U}^{92+}$ at maximum	bare ions up to Z = 28 $\text{Kr}^{34+}, \text{Xe}^{48+}, \text{Au}^{60+}$, etc.
setup time	≥ 1 day	hours
remarks	large devices liquid helium cooling latest developments: refrigerator cooling	compact, transportable, low initial and maintenance costs, short setup times

2.2 The EBIS History: A Short Retrospect

For about 20 years EBIT/EBIS ion sources have now been available as reliable sources of HCIs. After the first demonstration of the working principle of an electron beam ion source (EBIS) in the pioneer works of Donets, Ovsyannikov and collaborators [9–11] the development of a first compact electron beam ion trap (EBIT) was reported by Levine et al. [12]. Starting with this date a manyfold of different EBIT/EBIS ion sources has been developed and put into operation at different places all over the world.

Before all it seems to be necessary to clear up the terms "EBIT and "EBIS". Both terms can be found in the literature. The term EBIT stands for Electron Beam Ion Trap. Since all EBIT can principally

also work like an EBIS it seems to be more common to speak about EBIS unless the function as ion trap is of interest as this is the case in spectroscopic studies on HCIs.

Making no claim to be complete sources such as the LLNL EBIT, the NIST EBIT, the Tokyo EBIT, the Shanghai EBIT and the Heidelberg EBIT with their different modifications should be named here. Furthermore, first activities to built a refrigerated (cryogenic closed cycle, no liquid helium) EBIT with a 2 cm ion trap using outer correction coils are known [18] and were realized with the Stockholm EBIT. Most of these EBIs are special constructions realized by several laboratories with the goal to perform specific investigations on highly charged ions.

Another development line is the series of compact room-temperature EBIT/EBIS ion sources of the Dresden EBIT/EBIS family [14, 15]. They have a patented operation principle which allows for producing highly charged ions efficiently and with ion beam currents competitive to other known EBIT/EBIS solutions. Continuing this way a new refrigerated superconducting ion source, the Dresden EBIS-SC, was constructed and commissioned in 2010 [16]. In this context the basic idea was to built up an ion source working with a liquid-helium-free refrigerator techniques for cooling the superconductors which generate the strong magnetic field compressing the electron beam and to realize a very compact design of the source body. In spite of the compact ion source assembly the system was proven for source operation with electron beams up to 700 mA.

An overview of EBIS installations in 2010 and earlier can be found in [17]. Nevertheless, the number of employed EBIS/EBIT is increasing permanently. In the last two years installations in Kielce and Krakow (both Poland), Huddersfield (Great Britain), Clemson (USA), Dresden-Rossendorf and Jena (both Germany) and Shanghai (China) have emerged.

Most of the EBIS of international reputation are special laboratory constructions, where each EBIS has its own particularities. Commercial versions of EBIT and EBIS devices are known only from two vendors:

- **Physics & Technology (Livermore/USA).**

Offered is a so-called REBIT/S (Refrigerated Electron beam Ion Trap / Source; for details see [18]).

- **Dreebit GmbH (Dresden/Germany).**

Offered is a series of compact and efficient room-temperature EBIT and EBIS sources (Dresden EBIT, Dresden EBIS and Dresden EBIS-A) as well as a superconducting EBIS (Dresden EBIS-SC), using refrigerating technology for magnet cooling (for details see [15]).

3 EBIS: The Basic Physics

3.1 The Ionization Balance

The intended purpose of an EBIS is to produce highly charged ions. To produce HCIs a high-density electron beam acts as ionization medium. For neutrals and ions in the electron beam the balance between

- charge generating processes and
- charge destructive processes

is of importance for reaching a certain ionization stage.

For ion production the dominant process is electron impact ionization. Therefore, only this process is considered at first. For the ion production in an EBIS we can write

$$\begin{aligned}
 \text{to } q=1 \quad \frac{dn_0}{dt} &= -\lambda_1 n_0 \\
 \vdots &\vdots \vdots \\
 \text{to } q \quad \frac{dn_q}{dt} &= \underbrace{\lambda_q n_{q-1}}_{\text{ion production}} - \underbrace{\lambda_{q+1} n_q}_{\text{ion destruction}} \\
 \vdots &\vdots \vdots \\
 \text{to } Z \quad \frac{dn_Z}{dt} &= \lambda_Z n_{Z-1}
 \end{aligned} \tag{2}$$

with n_0 – neutral particle density. For λ_q it holds

$$\lambda_q = \sigma_q v_e n_e \quad (\text{reaction rate}) \tag{3}$$

λ_q has the dimension of 1/s and σ_q – ionization cross-section, v_e – electron velocity and n_e – electron density.

If the ionization process starts only with neutral particles it yields

$$t = 0; \quad n_0(0) = n_0^0; \quad n_q(0) = 0.$$

This leads to the solution

$$\begin{aligned}
 n_0 &= n_0^0 e^{-\lambda_1 t} \\
 n_1 &= \frac{n_0^0 \lambda_1}{\lambda_2 - \lambda_1} \left(e^{-\lambda_1 t} - e^{-\lambda_2 t} \right) \\
 n_2 &= n_0^0 \lambda_1 \lambda_2 \left(\frac{e^{-\lambda_1 t}}{(\lambda_2 - \lambda_1)(\lambda_3 - \lambda_1)} + \frac{e^{-\lambda_2 t}}{(\lambda_3 - \lambda_2)(\lambda_1 - \lambda_2)} + \frac{e^{-\lambda_3 t}}{(\lambda_1 - \lambda_3)(\lambda_2 - \lambda_3)} \right) \\
 \vdots &\vdots \\
 n_q &= n_0^0 \prod_{l=1}^q \lambda_l \left(\sum_{j=1}^{q+1} \frac{e^{-\lambda_j t}}{\prod_{k=1, k \neq j}^{q+1} (\lambda_k - \lambda_j)} \right)
 \end{aligned} \tag{4}$$

In principle, equation (2) can also be integrated for other conditions as for example for $n_q(0) \neq 0$, for charge breeding processes or for external ion injection into an EBIS.

With equation (3) the production rate of ions with individual ion charge states can be determined.

If we develop the exponents in equation (4) it yields

$$\begin{aligned}
 n_0 &= n_0^0 (1 - \lambda_1 t) \\
 n_1 &= n_0^0 \lambda_1 t \\
 n_2 &= n_0^0 \lambda_1 \lambda_2 \frac{t^2}{2} \\
 &\vdots \quad \vdots
 \end{aligned} \tag{5}$$

$$n_q = n_0^0 \frac{t^q}{q!} \prod_{j=1}^q \lambda_j.$$

The characteristic time τ for ion production (ionization time) follows using

$$t_q = \frac{1}{\lambda_q} = \frac{1}{\sigma_q v_e n_e} \left(\frac{1}{\text{reaction rate}} \right) \quad (6)$$

to

$$\begin{aligned} \tau_1 &= t_1 \\ \tau_2 &= t_1 + t_2 \\ &\vdots && \vdots \\ \tau_q &= \sum_{k=1}^q t_k \end{aligned} \quad (7)$$

For the estimation when a certain ionization stage reaches its maximum in the actual ion charge state distribution equation (7) can be used. Hence we write

$$j_e \tau_q = \sum_{k=1}^q \frac{e}{\sigma_k} \quad (\text{ionization factor}) \quad (8)$$

with

$$j_e = n_e v_e$$

as electron beam density (in A/cm²). The ionization factor is a fundamental quantity which determines the ionization stage in an ion source.

The production of a mean ion charge state \bar{q} is only possible if a certain $j\tau$ value (ionization factor) is reached. It must apply

$$j_e \tau_q \geq \sum_{k=1}^q \frac{e}{\sigma_k} \quad (9)$$

Precondition must be an electron energy E_e higher than the ionization potential I_q (ideally about $(2\dots 3) \cdot I_q$).

The best values for the ionization factor and the electron beam energy under consideration of the excitation function of the electron-impact ionization cross sections for selected elements are shown in Fig. 4. Thus producing high ionization stages requires

- a sufficiently electron beam energy and
- a sufficiently high ionization factor.

In order to explain the role of electron binding energies in Fig. 5 in more detail we show the electron binding energies of ions for different isoelectronic sequences as a function of the atomic number. Thereby it is considered that the ionization cross-section has its maximum at about 2.7-times of the electron binding energy of the electron to be ionized.

Figure 6 shows this behaviour for xenon ions. The ionization factor for the production of a certain ion charge state is minimal at 2.7-times the electron binding energy and increases again at higher electron energies. To produce highest ionization charge states ionization factors many orders of magnitude higher than those ones for low charged ions must be reached. It should be noted again that the issues discussed are only valid under the idealized condition that only electron impact ionization takes place.

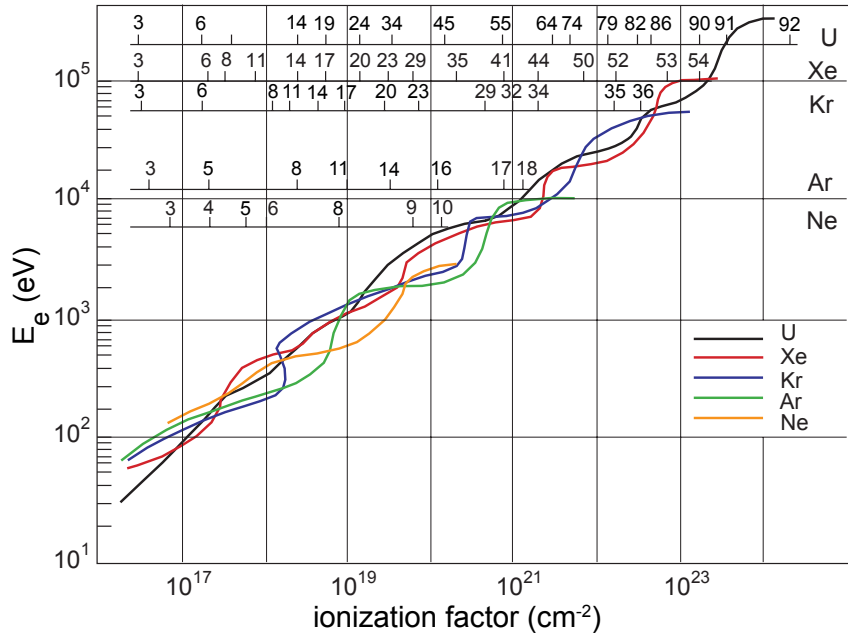


Fig. 4: Interrelation between ionization factor and electron energy for the effective production of ions in different ion charge states (according to an idea of Prof. E.D.Donets (Dubna).

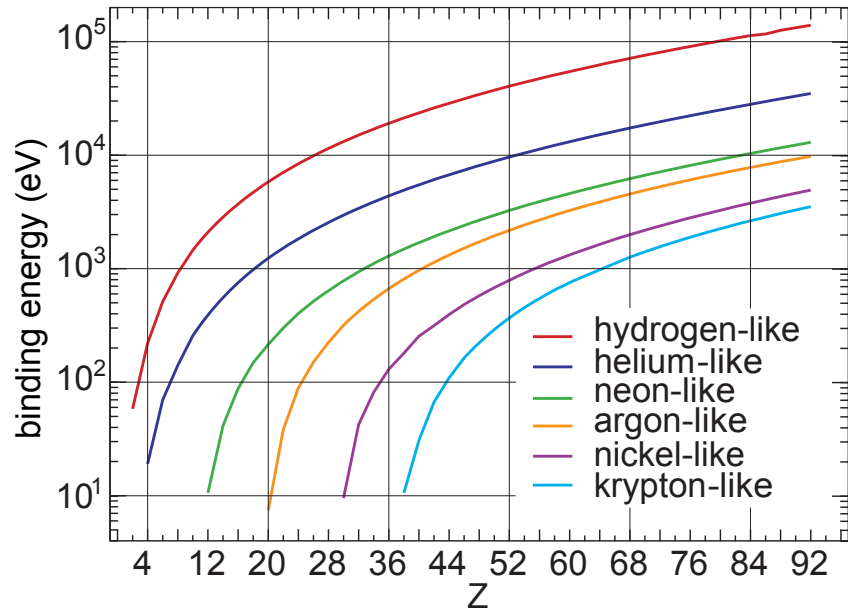


Fig. 5: Electron binding energies for the ion production of different isoelectronic sequences.

In practice processes such as

- charge exchange and
- ion losses from the source

can reduce the ionization power significantly. Of special importance in this case is the charge exchange with neutrals. The ionisation factor in dependence on the ionization time and the electron energy for selected isoelectronic sequences is given in Table 2 (according to [19]).

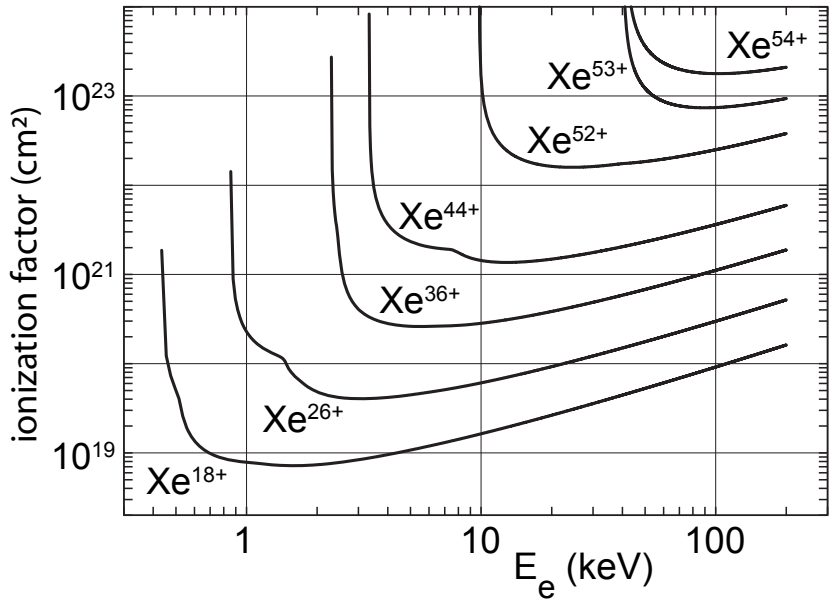


Fig. 6: Ionization factors for the production of individual xenon ionization charge states.

3.2 Atomic Physics for Ion Production

3.2.1 Overview

Atomic processes contributing to the ion production are

1. electron impact ionization,
2. charge exchange,
3. recombination,
4. three-body recombination,
5. dielectronic recombination,
6. photoionization,
7. vacancy cascades and
8. electron shake-off processes.

Later on we will discuss processes important for ion losses and the energy balance in EBIS:

- ion heating by elastic electron collisions,
- ion-ion energy exchange,
- ion confinement and
- ion losses from the trap.

In the following we will discuss the most important processes in more detail. For the basic atomic processes some useful estimation formula are given. Nevertheless, we note that these formula do not completely substitute more precise quantum mechanical calculations of individual processes.

3.2.2 Direct Coulomb Ionization

In simple case the cross-sections for single electron impact ionization

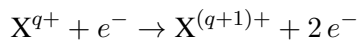


Table 2: Ideal production conditions for ions of different isoelectronic sequences. Given is the ionization factor $j_e \tau$ [$\text{e}^- \text{cm}^{-2}$], the optimal electron beam energy and the required ionization time for an assumed ionization factor of $j_e \tau = 3 \cdot 10^{22} \text{ e/cm}^2$.

sequence	neon Z=10	argon Z=18	krypton Z=36	xenon Z=54	gold Z=79	uranium Z=92
atom fully ionized	Ne^{10+} $2 \cdot 10^{21}$ 3 keV 7 ms	Ar^{18+} $2 \cdot 10^{21}$ 9 keV 67 ms	Kr^{36+} $3 \cdot 10^{22}$ 40 keV 1 s	Xe^{54+} $2 \cdot 10^{23}$ 80 keV 7 s	Au^{79+} $6 \cdot 10^{23}$ 180 keV 20 s	U^{92+} $2 \cdot 10^{24+}$ 300 keV 67 s
helium-like	Ne^{8+} $8 \cdot 10^{18}$ 0.6 keV 0.3 ms	Ar^{16+} $1 \cdot 10^{20}$ 2 keV 3 ms	Kr^{34+} $2 \cdot 10^{21}$ 7 keV 67 ms	Xe^{52+} $2 \cdot 10^{22}$ 20 keV 0.7 s	Au^{77+} $6 \cdot 10^{22}$ 45 keV 2 s	U^{90+} $2 \cdot 10^{23}$ 70 keV 7 s
neon-like		Ar^{8+} $3 \cdot 10^{18}$ 0.3 keV 0.1 ms	Kr^{28+} $3 \cdot 10^{20}$ 4 keV 10 ms	Xe^{44+} $2 \cdot 10^{21}$ 8 keV 67 ms	Au^{69+} $6 \cdot 10^{21}$ 17 keV 200 ms	U^{82+} $3 \cdot 10^{22}$ 30 keV 1 s
argon-like			Kr^{18+} $1 \cdot 10^{19}$ 1.5 keV 0.3 ms	Xe^{36+} $2 \cdot 10^{20}$ 5 keV 7 ms	Au^{61+} $1 \cdot 10^{21}$ 12 keV 33 ms	U^{74+} $5 \cdot 10^{21}$ 20 keV 167 ms
krypton-like				Xe^{18+} $6 \cdot 10^{18}$ 1 keV 0.4 ms	Au^{43+} $1 \cdot 10^{20}$ 4 keV 3 ms	U^{56+} $7 \cdot 10^{20}$ 7 keV 23 ms
xenon-like					Au^{25+} $2 \cdot 10^{19}$ 1.5 keV 0.7 ms	U^{38+} $7 \cdot 10^{19}$ 4 keV 2 ms

can be estimated for different subshells j by the Lotz formula [20]

$$\sigma_{qj} = a_{qj} g_{qj} \frac{\ln \frac{E_e}{I_{qj}}}{E_e I_{qj}} \left\{ 1 - b_{qj} \exp \left[-c_{qj} \left(\frac{E_e}{I_{qj}} - 1 \right) \right] \right\} \quad (10)$$

For all ionization processes the electron energy E_e must be greater than the related ionization potential I_{qj} , otherwise the ionization cross-section is equal to zero.

The quantities a_{qj}, b_{qj} and c_{qj} are tabulated constants. For highly charged ions they are given according to

$$a_{qj} = 4,5 \cdot 10^{-14} \text{ cm}^2 \text{ eV}^2$$

$$b_{qj} = c_{qj} = 0$$

with g_{qj} as occupation number of the subshell j of an ion in the charge state q . I_{qj} describes the ionization potential for the ionization of the subshell j .

The total ionization cross-section results as a sum over all occupied subshells

$$\sigma_q(E_e) = \sum_q \sigma_{qj}(E_e) \quad (11)$$

As an example electron impact ionization cross-sections for argon ions are shown in Figure 7.

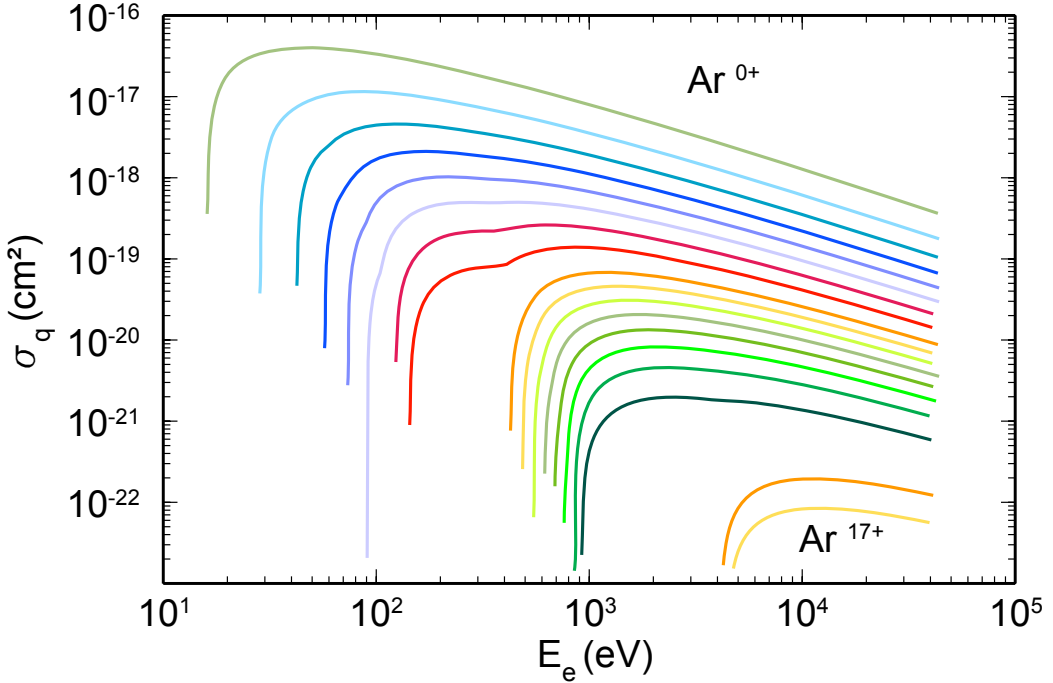


Fig. 7: Single electron impact ionization cross-sections as a function of the electron energy (according to [21]).

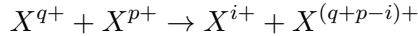
For the double ionization process



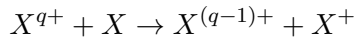
we wont go into details but we refer to the estimation formula from Mueller and Frodel [22] which was derived from experimental data. As a rule double ionization cross-sections for the most species are about one order of magnitude or more lower than cross-sections from single ionization cross-sections.

3.2.3 Charge Exchange

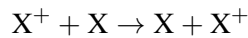
For the charge exchange between ions it yields



and correspondingly for the charge exchange with a neutral atom



Due to



for singly charged ions charge exchange does not play a role.

Of special importance in this case is the charge exchange of ions with neutrals due to the very high cross-sections. This circumstance is important for the EBIS operation and can limit the reachable ionization stages in the electron beam.

For collision energies below 25 keV/u charge exchange can be estimated by the formula (Mueller and Salzborn [23])

$$\sigma_{q \rightarrow q-1} [\text{cm}^2] \approx (1,43 \pm 0,76) \cdot 10^{-12} q^{1,17} (I_q [\text{eV}])^{-2,76} \quad (12)$$

and is in the order of $10^{-14} \dots 10^{-15} \text{ cm}^{-2}$. As a rule the charge exchange is the dominant loss mechanism for highly charged ions and is especially important if the gas pressure in the ion source is relatively high. As we see from equation 12 the cross-section is independent on the energy of the projectiles. In Fig. 6 cross-section for single and double charge exchange are given for xenon ions.

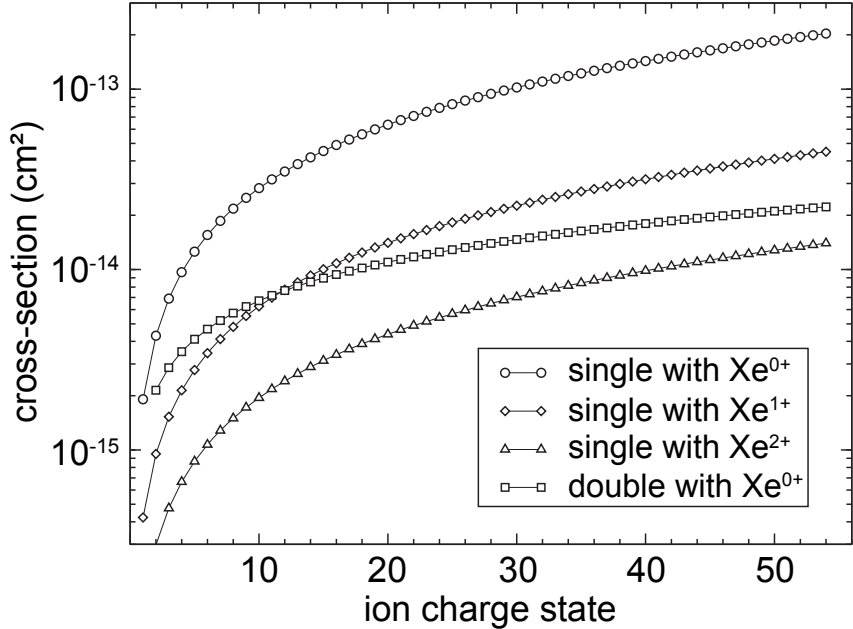
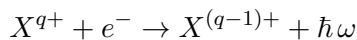


Fig. 8: Charge exchange cross-sections for single charge exchange with $\text{Xe}^{(0,1,2)}$ ions as well as for the double charge exchange with xenon neutrals (after [24])

3.2.4 Radiative Recombination

The scheme of the Radiative Recombination (RR)



is shown in Fig. 3.2.4.

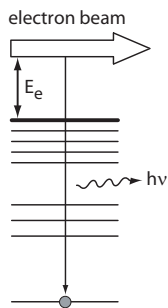


Fig. 9: Scheme of the Radiative Recombination process. The energy $\hbar\omega$ of the emitted photon calculates to $\hbar\omega = E_e - E_B$.

The cross-section for charge exchange processes can be estimated by the formula from KIM and PRATT [25]

$$\sigma_q^{RR}(E_e) = \frac{8\pi}{3\sqrt{3}} \alpha \lambda_e^2 \chi_q(E_e) \ln \left(1 + \frac{\chi_q(E_e)}{2\hat{n}} \right) \quad (13)$$

with

$$\chi_q(E_e) = (Z + q)^2 \frac{I_H}{4 E_e}$$

and

$$\hat{n} = n + (1 - W_n) - 0, 3$$

Here n is the main quantum number of the valence shell, W_n ratio of the number of unoccupied states to the total number of states in the valence shell, $\lambda_e = 3,861 \cdot 10^{-11} \text{ cm}$ (electronic Compton wavelength) and $I_H = 13,6 \text{ eV}$.

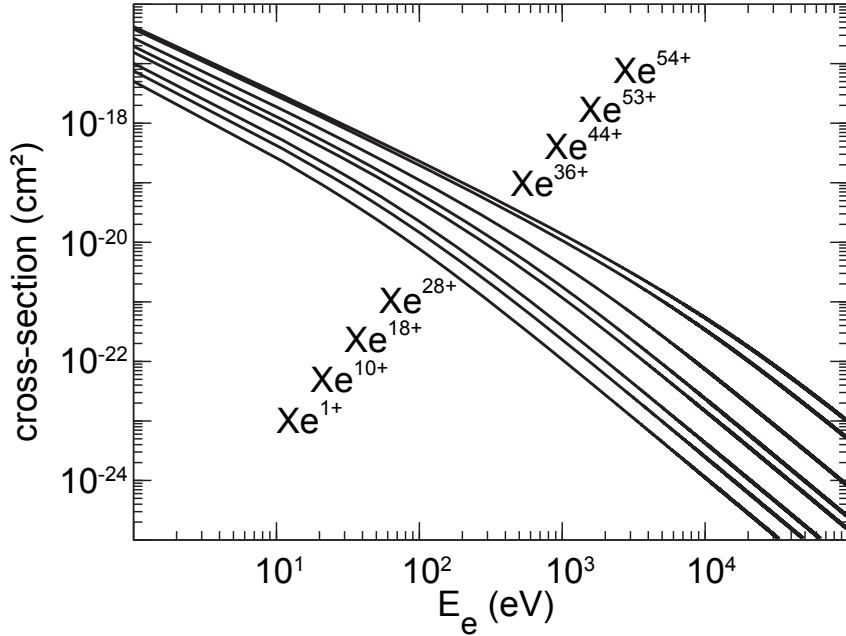


Fig. 10: Cross-sections for the Radiative Recombination on xenon ions (according to [24])

As example we show the cross-sections for the Radiative Recombination on xenon ions as a function of the electron energy in Fig. 10.

Since RR processes counteract to the ionization for each element and ion charge state there exist a characteristic electron energy when the ionization rate is equal to the RR rate. This behaviour is discussed in more detail in [26].

3.2.5 Further Processes

Beside the discussed main processes in special cases further contributions from

- Dielectronic Recombination (DR),
- three body recombination,
- vacancy cascades and
- photoionization

are of interest but should not be discussed here.

3.3 Balance Equation for the Ion Charge State Distribution

The number of ions with the charge q produced from ions with the charge $(q - 1)$ and ionized further to the charge state $(q + 1)$ can be described by a balance equation for successive electron impact ionization

and competing processes

$$\begin{aligned}\frac{dn_q}{dt} = & R_{q-1 \rightarrow q}^{ion} - R_{q \rightarrow q+1}^{ion} + R_{q+1 \rightarrow q}^{RR} - R_{q \rightarrow q-1}^{RR} \\ & + R_{q+1 \rightarrow q}^{exch} - R_{q \rightarrow q-1}^{exch} - R_q^{ax,esc} - R_q^{rad,esc} + R_q^{source}\end{aligned}\quad (14)$$

with

R^{ion}	- ionization terms
R^{RR}	- terms for Radiative Recombination
R^{exch}	- Charge Exchange terms
$R^{ax,esc}$	- terms for axial ion losses
$R^{rad,esc}$	- terms for radial ion losses
R^{source}	- particle source term

If the ionization process occurs in single step processes and if we neglect the axial loss (which is a good approximation for appropriate field configurations) it yields

$$\begin{aligned}\frac{dn_0}{dt} = & \underbrace{-n_o \lambda_{0,1}}_{\text{ionization}} + \underbrace{n_1 \lambda_{1,0}}_{\text{Charge Exchange}} \\ \frac{dn_1}{dt} = & n_o \lambda_{0,1} - n_1 (\lambda_{1,2} + \lambda_{1,0}) + n_2 \lambda_{2,1} - \left[\frac{dn_1}{dt} \right]^{rad,esc} \\ \vdots & \vdots \vdots \\ \frac{dn_q}{dt} = & n_{q-1} \lambda_{q-1,q} - n_q (\lambda_{q,q+1} + \lambda_{q,q-1}) + n_{q+1} \lambda_{q+1,q} - \left[\frac{dn_q}{dt} \right]^{rad,esc} \\ \frac{dn_z}{dt} = & n_{Z-1} \lambda_{Z-1,Z} - n_Z \lambda_{Z,Z-1} - \left[\frac{dn_Z}{dt} \right]^{rad,esc}\end{aligned}\quad (15)$$

Here $n_0 \dots n_Z$ are the densities for neutrals and ions of the charge state q . Further we have

$\lambda_{q,q+1}$	- ionization coefficient
$\lambda_{q,q-1}$	- recombination and charge exchange coefficients.

Details about the corresponding terms, the influence on the development of the individual ion densities, the development of the energy densities and ion evaporation of ions from the ionization volume can be found for example in [27, 28].

In Fig. 11 we exemplarily show the time development of the ionization of xenon ions in the electron beam of a Dresden EBIT as it follows from equation system (14).

3.4 Ion Source Physics: Selected Topics

Due to the restricted scope of this report only some information about important (but not complete) details of EBIS are given. For more detailed studies please refer to corresponding literature. Due to simplicity and copyright items the author will give in the following examples of results from EBIS of the Dresden EBIS type.

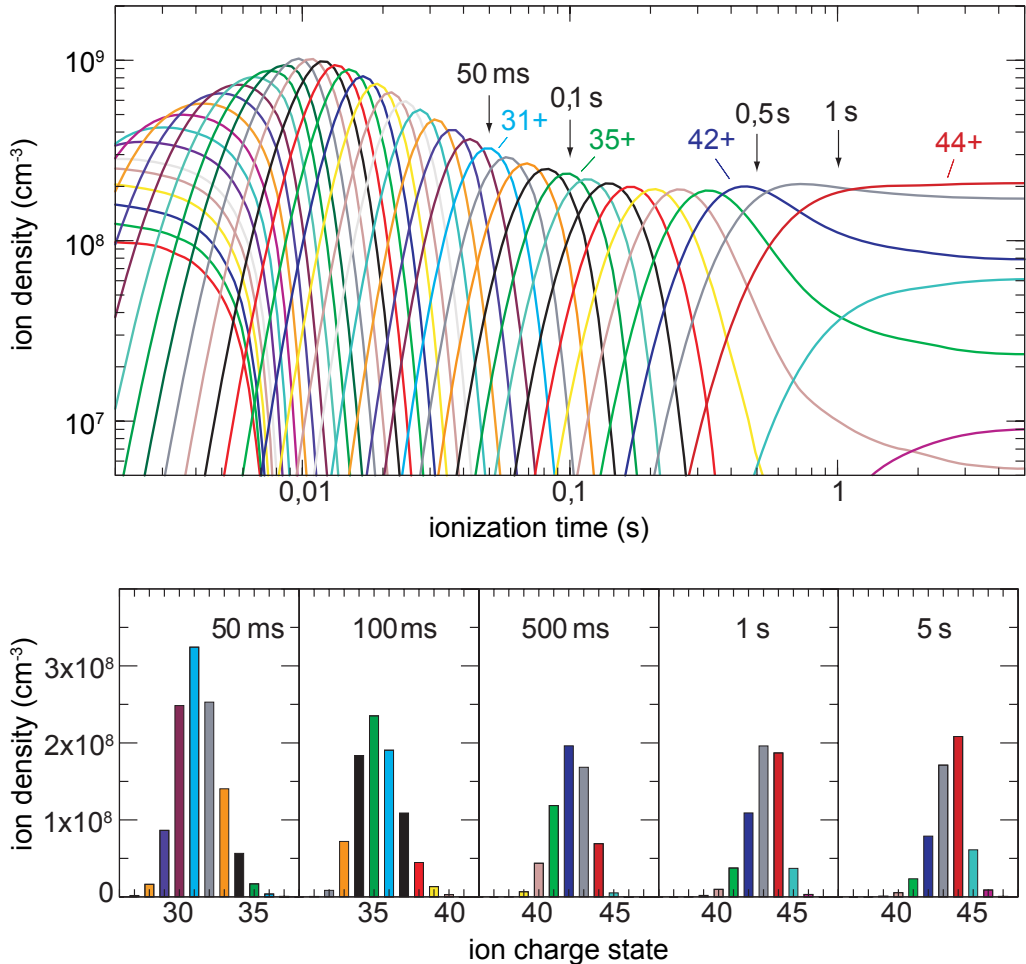


Fig. 11: Evolution of the ionization of xenon ions in a Dresden EBIT at $E_e = 15$ keV, $I_e = 40$ mA and $p = 2 \cdot 10^{-9}$ mbar.

3.4.1 Electrical Trap Capacity

The ion trapping in an EBIS (see Fig. 12) occurs

- in axial direction by electrostatic potentials and
- in radial direction by the space charge potential of the electron beam.

The total number of ions that can be stored in an EBIS is limited by the electrical trap capacity C_{el} . For an estimation of C_{el} we assume a homogeneous electron beam which passes an ion trap of the length L with the electron beam current I_e and an electron energy E_e . Then the number of negative charges in the beam volume is a measure for the trap capacity C_{el} . With

$$I_e = \frac{dQ}{dt}, \quad v_e = \frac{dx}{dt}, \quad v_e = \sqrt{\frac{2E_e}{m_e}}$$

we have

$$\Delta Q = \frac{I_e \Delta x}{v_e} = \frac{I_e L}{\sqrt{\frac{2E_e}{m_e}}}$$

and for the trap capacity

$$C_{el} = 1,05 \cdot 10^{13} \frac{I_e [\text{A}] L [\text{m}]}{\sqrt{E_e [\text{eV}]}} \quad (16)$$

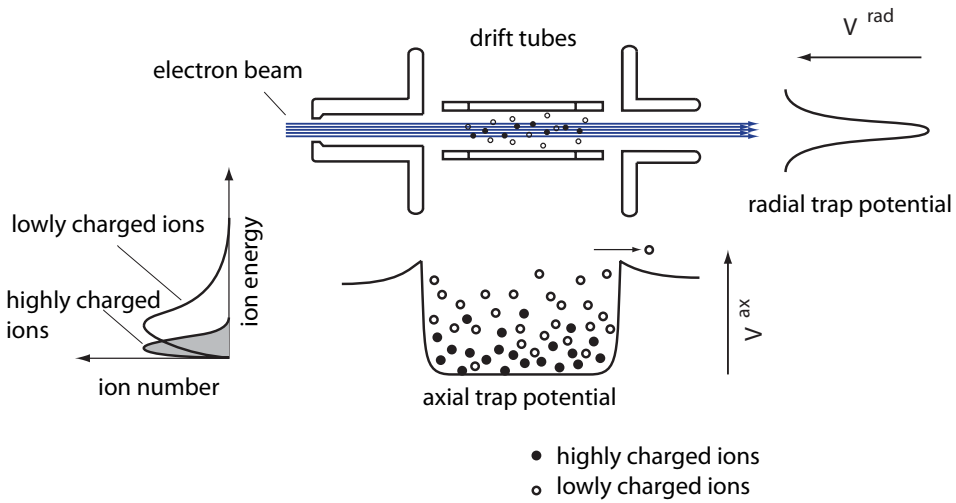


Fig. 12: Axial and radial potentials in an EBIT. Due to the effective trap height according to $V_b \times q$ highly charged ions are trapped stronger than lowly charged ones. The energy exchange between the ions leads to an equilibrium distribution of the ion energy.

In order to estimate the useable trap capacity in practice we must supplement equation (16) to

$$C_{el} = 1,05 \cdot 10^{13} \frac{I_e [\text{A}] L [\text{m}]}{\sqrt{E_e [\text{eV}]}} \alpha f \quad (17)$$

with α – ratio of ions with a certain ion charge state in the ion charge state distribution and f – charge compensation of the electron beam.

3.4.2 Boltzmann Distribution of the Ion Energy

In the source volume ion-ion collisions lead very fast (in about ms) to a Boltzmann distribution of the ion energy

$$f(E_i) = \frac{2}{\sqrt{\pi} k T_i} \sqrt{\frac{E_i}{k T_i}} e^{-\frac{E_i}{k T_i}} \quad (18)$$

The formation of a Boltzmann energy distribution has consequences for the whole ion trap process:

- **Permanent ion losses.** At a certain mean ion energy always ions exist with an energy greater than a critical energy

$$E_{kr} = q U_b \quad (19)$$

and which can leave the trap with the barrier U_b . This means we have a constant ion loss from the trap. The ion loss ratio can be derived by integrating the distribution function. The behaviour of ions in the trap can be described by the nonstationary Boltzmann equation in a self-consistent model considering ionization and energy exchange processes.

- **Evaporation cooling** of multiply charged ions by light LCIs. Elastic collisions between ions with different charge states and masses lead to an equilibrium energy distribution for each ion sort. Thereby the critical energy for leaving the ion trap for LCIs is lower than for highly charged ions, i.e. the ion living time in the ion trap is lower for LCIs. LCIs leave the beam first, i.e. they evaporate and transport the energy transmitted from the highly charged ions to lower charged ones out of the ionization volume. As result of the process the mean temperature of the highly charged ions decreases and ion losses of these ions are reduced.

3.4.3 Radial Trap Potential

For simplicity we consider an ion trap with an radial symmetric electron beam which electron density is homogenous distributed over the radius r_e of the electron beam. Using the Gauss theorem the radial trap potential has the shape

$$V_e(r) = \begin{cases} \frac{U_e r^2}{r_e^2} & \text{for } r < r_e \\ U_e \left(2 \ln \frac{r}{r_e} + 1 \right) & \text{for } r > r_e \end{cases} \quad (20)$$

Here for U_e yields

$$U_e = \frac{I_e}{4\pi\varepsilon_0 v_e} = \frac{1}{4\pi\varepsilon_0} \sqrt{\frac{m_e}{2}} \frac{I_e}{\sqrt{E_e}} \quad (21)$$

We can estimate U_e with

$$U_e [\text{V}] = \frac{30 I [\text{A}]}{\sqrt{1 - \left(\frac{E_e [\text{keV}]}{511} + 1 \right)^{-2}}} \quad (22)$$

As example the radial trap potential in Fig. 13 is shown for an typical operation regime of a Dresden EBIT.

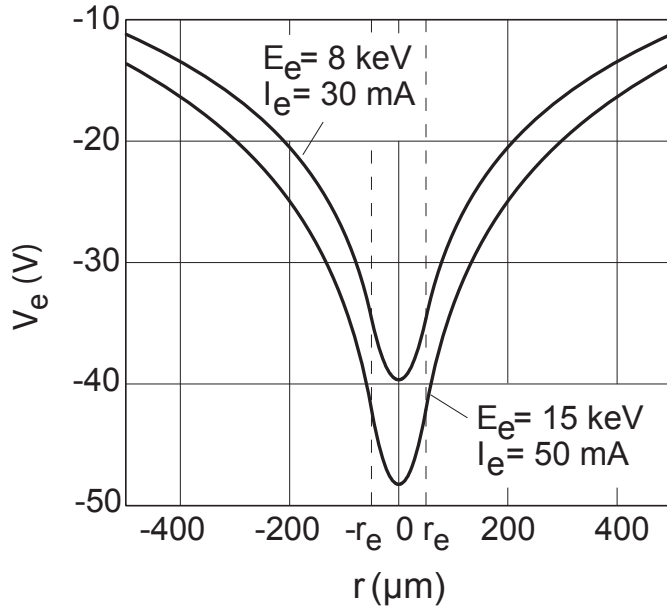


Fig. 13: Radial trap potential of a Dresden EBIT for two different electron beam currents.

The ion confinement is additionally influenced by the magnetic field enclosing the electron beam so that we finally have an effective radial potential of

$$V_e^{eff}(r) = V_e(r) + \frac{e q_i B^2 r^2}{8 m_i} \quad (23)$$

with R - drift tube radius.

3.4.4 Ion Heating and Energy Balance

Ions are heated in the electron beam by elastic Coulomb collisions and by microwave instabilities. If instabilities do not appear (huge Debye lenghts) the main heating processes are elastic electron-ion collisions.

Elastic electron-ion collisions. Ion heating by elastic electron collisions can be described by

$$\left[\frac{dE_i}{dt} \right]^{\text{heat}} = (n_i \sigma_i v_e) \left(2 \frac{m_e}{m_i} E_e \right) = 2 \frac{m_e}{m_i} E_e f_{ei} \quad (24)$$

with

$$t_{ei} = f_{ei}^{-1} = \frac{1}{n_i < v_e \sigma_i >}$$

and σ_i - Coulomb collision cross-section

$$\sigma_i = \frac{1}{(4\pi\varepsilon_0)^2} 4\pi \left(\frac{q_i e^2}{m_e} \right)^2 \frac{\ln \Lambda_{ei}}{v_e^4}$$

The Coulomb logarithm for electron-ion collisions $\ln \Lambda_{ei}$ has the shape

$$\ln \Lambda_{ei} = \begin{cases} 23 - \ln \frac{q_i \sqrt{n_e}}{(k T_e)^{3/2}} & \text{for } q_i^2 \cdot 10 \text{ eV} > k T_e > \frac{m_e}{m_i} k T_i \\ 24 - \ln \frac{\sqrt{n_e}}{(k T_e)} & \text{for } k T_e > q_i^2 \cdot 10 \text{ eV} > \frac{m_e}{m_i} k T_i \\ 30 - \ln \frac{q_i^2 \sqrt{n_e}}{(k T_i)^{3/2} A_i} & \text{for } k T_e < \frac{m_e}{m_i} q_i k T_i \end{cases} \quad (25)$$

with kT -Energy in eV, n - density in cm^{-3} , A_i - atomic mass and k - Boltzmann constant. Energy transfer by Coulomb collisions occur then with a rate

$$\left[\frac{d(n_i k T_i)}{dt} \right]^{\text{heat}} \approx \left(- \frac{dE_e}{dt} \right) n_e \quad (26)$$

Elastic ion-ion collisions. Energy transfer between ions occur by elastic ion-ion collisions. In these collisions energetic ("hot") ions are cooled by colder ions. If we assume a Boltzmann distribution of the ion energy the cooling process can be characterized by

$$\left[\frac{dE}{dt} \right]^{\text{exch}} = 2 \nu_{ij} n_i \frac{m_i}{m_j} \frac{k T_j - k T_i}{\left(1 + \frac{m_i T_j}{m_j T_i} \right)^{3/2}} \quad (27)$$

Here the ν_{ij} are Coulomb collision rates between the ions

$$\nu_{ij} = \frac{1}{(4\pi\varepsilon_0)^2} \frac{4\sqrt{2\pi}}{3} n_j \left(\frac{q_i q_j e^2}{m_i} \right)^2 \left(\frac{m_i}{k T_i} \right)^{3/2} \ln \Lambda_{ij} \quad (28)$$

with Λ_{ij} as Coulomb logarithm for ion-ion collisions

$$\ln \Lambda_{ij} = \ln \Lambda_{ji} = 23 - \ln \left[\frac{q_i q_j (m_i + m_j)}{m_i T_j + m_j T_i} \left(\frac{n_i q_i^2}{T_i} + \frac{n_j q_j^2}{T_j} \right)^{1/2} \right] \quad (29)$$

The energy transfer by ion-ion collisions is applied for the evaporative cooling where low charged ions cool down higher charged ions. As source for LCIs attends the rest gas in the source. Because ion-ion collisions occur very efficiently the ions tend to a thermal equilibrium. The energy the ions have leaving the ion trap is then proportional to the ion charge state. Important is to mention that there exist

an upper limit for the neutral gas density because otherwise the number of highly charged ions will be reduced dramatically by charge exchange processes.

The energy which is transferred out of the ion source by the evaporation process can be described by the cooling rate

$$\frac{dE_0}{dt} \left[\frac{\text{eV}}{\text{s cm}^3} \right] = \frac{dn_{\text{LCI}} [\text{cm}^{-3}]}{dt} U_b [\text{V}] q_{\text{LCI}} \quad (30)$$

with n_{LCI} - equilibrium density of the LCIs and q_{LCI} - ion charge state of the LCIs.

3.4.5 Electron Beam: Equation of Motion and Beam Radius

The equation of motion for the electron beam in the paraxial approximation can be written as

$$\frac{d^2r}{dt^2} = \frac{e I_e}{2\pi\varepsilon_0 v_z r m_e} + \frac{e^2}{4m_e^2} \left(\frac{B_c^2 r_c^4}{r^3} - B_z^2 r \right) \quad (31)$$

with B_c – B-field at the cathode, B_z – axial magnetic field, r_c – cathode radius, I_e – electron beam current and v_z – axial electron velocity.

If we assume $B_c = 0$ than there exists a stationary solution of equation (31). The solution corresponds to an equilibrium flow of the electrons with constant radius, the so-called Brillouin flow (index "B"). For a Brillouin flow all electrons have a constant distance to the beam center. Thereby the Lorentz force caused by the magnetic field is compensated by the space charge and the centrifugal force of the rotating electrons.

If we consider more realistic assumptions such as

- a magnetic field at the cathode,
- thermal effects at the cathode due to filament heating up to the temperature T_c and
- interactions between the electrons

then this leads to a corrected electron beam radius (smaller than r_B) as described by Herrmann [29].

According to the Herrmann theory the electron beam radius enclosing 80% of the beam calculates to [30]

$$r_e = r(0) \sqrt{\left(1 - \frac{r_0}{r(0)}\right)^2 + \frac{2}{1 + \frac{B_C^2 r_C^4}{B_z^2 r_0^4}} \left(\frac{v_e \tan \gamma}{e} B_z \gamma\right)}, \quad (32)$$

and

$$r_0 = r_B \left(\frac{1}{2} + \frac{1}{2} \left[1 + 4 \left(\frac{8kT_C r_C^2 m_e}{e^2 B_z^2 r_B^4} + \frac{B_C^2 r_C^4}{B_z^2 r_B^4} \right) \right]^{1/2} \right)^{1/2}. \quad (33)$$

with $r(0)$ – beam radius at the cathode and γ – angle deviation from the source axis.

Generally the electron beam diameter of an EBIT depends on the actual technical solution. Typical diameters are in the order of 40 μm up to about 200 μm . A classical method to measure the electron beam diameter in an EBIS is shown in Fig. 14 and is discussed in more detail in [31]. The idea is to measure the X-rays emitted from ions in the electron beam which is ionized or excited by electron impact. Through an aperture the X-rays are detected on a CCD chip and the evaluation of the measured intensity distributions allows it to determine the electron beam diameter.

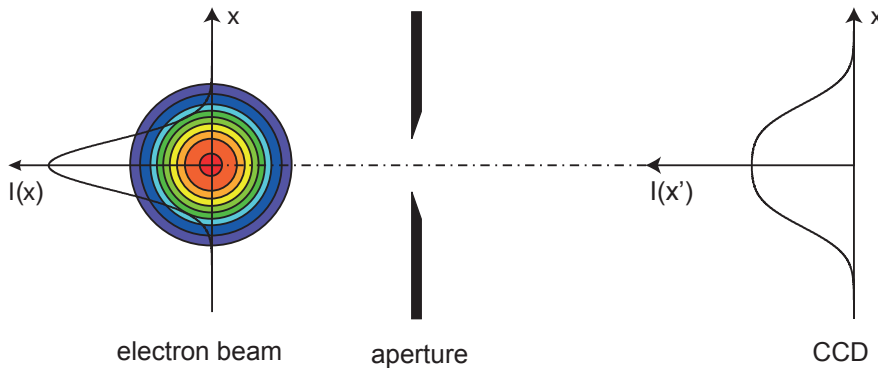


Fig. 14: CCD chip imaging of X-rays emitted from the electron beam (after [31]). $I(x)$ – x-ray intensity distribution from the electron beam, $I(x')$ – intensity distribution on the CCD

4 Ion Extraction from EBIS

4.1 Basic Ion Extraction Techniques

As mentioned before EBIS allow for production of ion beams in DC as well as pulsed mode. In the following we will discuss and characterize some basic features of EBIS ion extraction. If ions from an EBIS are applied in different experiments a basic problem is the separation of an individual ion charge state from the extracted ions which primarily contain a spectrum of individual ion charge states. Generally, the ion charge state separation is realized by

- magnetic dipole analyzers or
- Wien filters.

4.2 Ion Beam Separation using an Analyzing Magnet

A typical experimental setup for experiments with extracted ions and magnetic analysis of the ion charge states is shown in Fig. 15.

The facility shown in Fig. 15 was designed for experiments with highly charged ions for ion-solid interactions, atomic physics, biophysics, plasma physics, materials analysis, solid state physics etc. The ion source as well as the ion beamline can be insulated from ground potential. Thus ions with a wide range of kinetic energies (decelerated as well as accelerated) can be used for experiments in the target chamber of the facility which can be subdivided into 4 functional units, the ion source (for example Dresden EBIS-A), the first and the second beamline segment and the target chamber.

An einzel lens and an x-y-deflector as well as an aperture, a four jaw slit system and a Faraday cup are integrated in the first beamline segment. The einzel lens and the x-y-deflector are used to focus, deflect, and align the ion beam. An aperture with variable diameters can be used reducing the phase space of the ion beam and therefore improving the beam quality at the expense of beam intensity. A Faraday cup is used for detecting and measuring the ion beam current. It is mounted onto a translational feedthrough directly behind the four jaw slit system which is positioned in the focal point of the dipole magnet. Thus the determination of the beam position as well as the beam size is possible.

The ion beam extracted from the ion source can consist of ions of various elements and ion charge states. Thus a dipole magnet separates the ions according to their momentum in the second beamline segment. The momentum of the ion depends on the charge state and the mass of the ion. Hence ions with a certain charge-to-mass ratio can be selected.

The momentum-separated ions are aligned and deflected with a second x-y deflector positioned behind the dipole magnet. A second Faraday cup mounted in the focal point downstream of the dipole magnet ensures detection and current measurement of the ion beam using an electrometer.

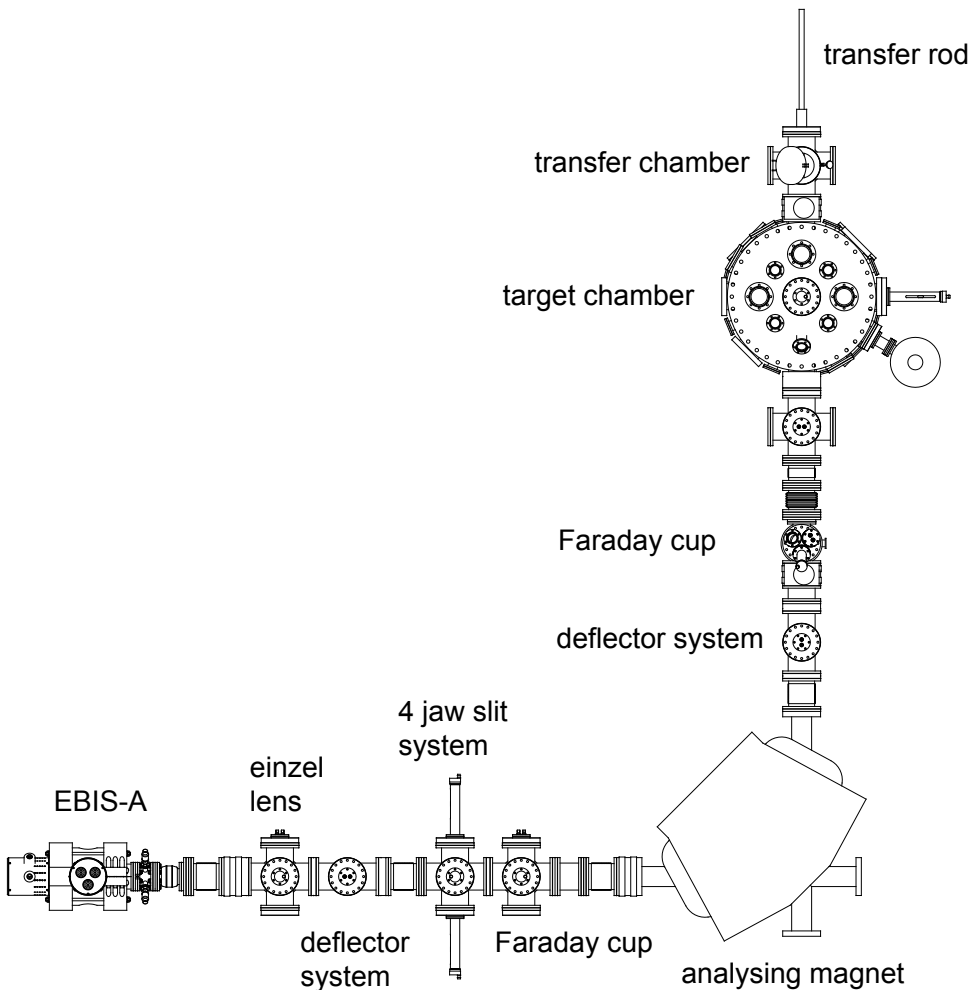


Fig. 15: Footprint of an ion beam facility featuring a Dresden EBIS-A including a 90 degree bending magnet for mass to charge ratio separation of the ion beam extracted from the EBIS.

The last functional unit of the facility consists of a deceleration lens and the target chamber. The ions are focused into the target chamber by the deceleration lens system. In principle it is possible to decelerate the ions down to a few eV as well as to accelerate them up to some tens of keV 40 keV per charge state. In the shown example the target chamber has two stages, an upper one for target irradiation experiments and a lower one for target preparation and target transfer. The upper stage is mounted onto the deceleration lens system. The target can be rotated (360°) and transferred via sample holder mounted to a 4-axes manipulator. The target can be heated by resistive heating as well as electron bombardment and cooled down via liquid nitrogen. With a wobble stick a further target manipulation inside the target chamber is possible. Measuring the beam intensity in the target chamber a third Faraday cup is mounted onto the 4 axes manipulator below the sample holder. A large number of vacuum ports allow the installation of various devices for experiments.

To characterize ion extraction spectra with an analyzing magnet some examples for ion extraction spectra are given as they can be expected for EBIS. Fig. 16 shows a xenon ion extraction spectrum as measured with a Dresden EBIS-A for an ionization time of 5 s. In Fig. 17 a carbon ion extraction spectrum is shown as measured with a superconducting Dresden EBIS-SC for an ionization time of 200 ms (for details see [32]).

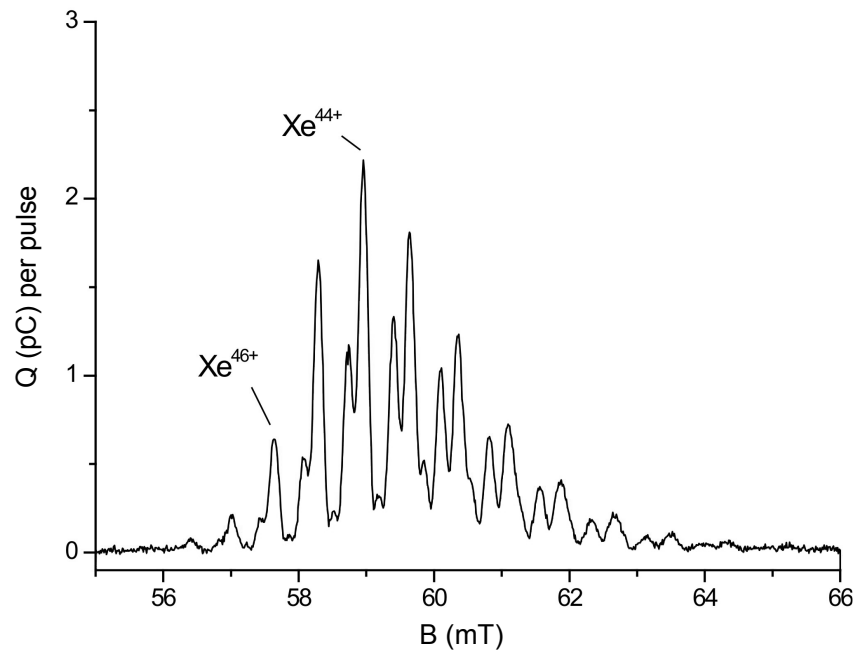


Fig. 16: A xenon ion extraction spectrum measured at an Dresden EBIS-A for a vacuum of 5×10^{-10} mbar, an electron beam energy of 12 keV and an electron beam current of 100 mA.

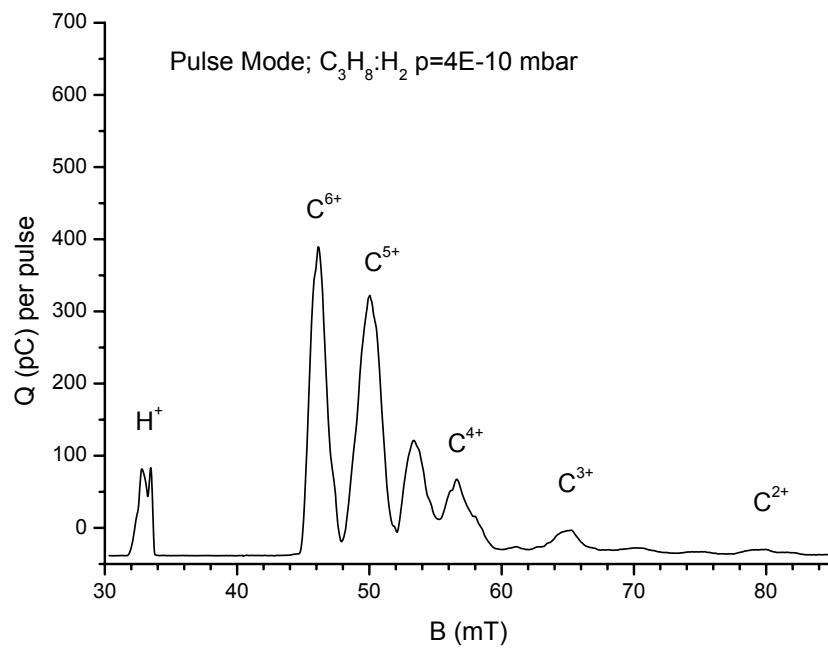


Fig. 17: A carbon ion extraction spectrum measured at an Dresden EBIS-SC for a vacuum of 4×10^{-10} mbar, an electron beam energy of 12 keV, an electron beam current of 400 mA and an ionization time of 200 ms.

4.3 Ion Beam Separation using a Wien Filter

A Wien Filter is a particle separator with a crossed magnetic and electric field configuration providing mass and charge state separated beams of excellent quality and small spatial dimensions [33]. With the Wien filter as an ion source add-on a very compact device is available substituting a complete standard beamline setup with a space consuming dipole magnet and other necessary equipment (see Fig. 18). The Wien filter can be used as stand-alone solution for various beam line setups. In dependence on the installed mass- and charge state-separating aperture a resolution of better than 80 is available. The geometrical dimensions of the Wien filter are small compared to a classical dipole magnet. The Wien filter fits easily on a beam line making a change of the ion beam direction obsolete, as it is necessary for a dipole magnet.

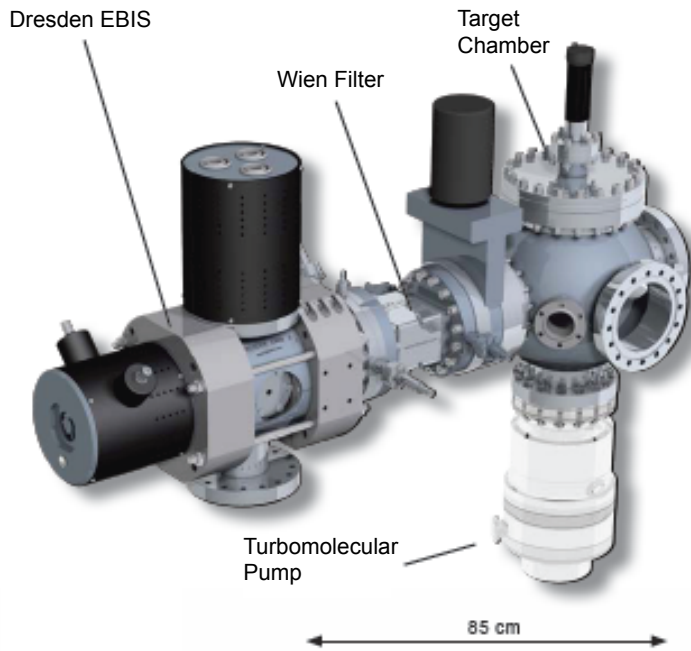


Fig. 18: A 3D presentation of a Wien filter based beamline.

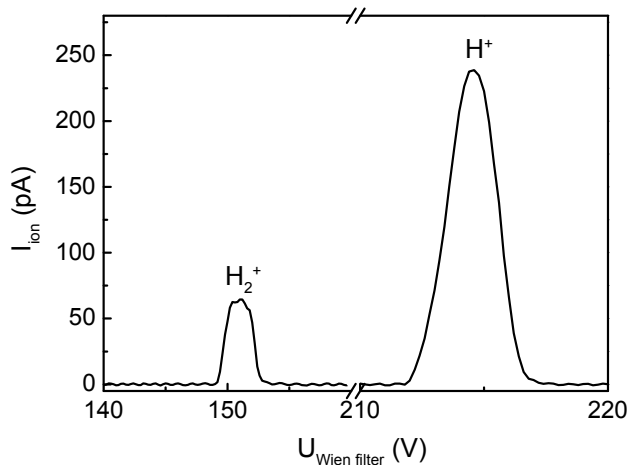


Fig. 19: A leaky mode hydrogen ion extraction spectrum measured at a Dresden EBIS for a vacuum of 3×10^{-9} mbar, an electron beam energy of 13.6 keV and an electron beam current of 30 mA.

The use of a Wien filter allows for separation of light and intermediate- Z ions of all ion charge states. For hydrogen and xenon this is shown in Fig. 19 and 20. The most important difference to the use of analyzing magnets is that a magnet has a gap of several centimeters, but for obtaining high resolution with a Wien filter we must work with aperture diameters in the millimetre or sub-millimetre region, i.e. beam losses through the Wien filter have to be taken into account.

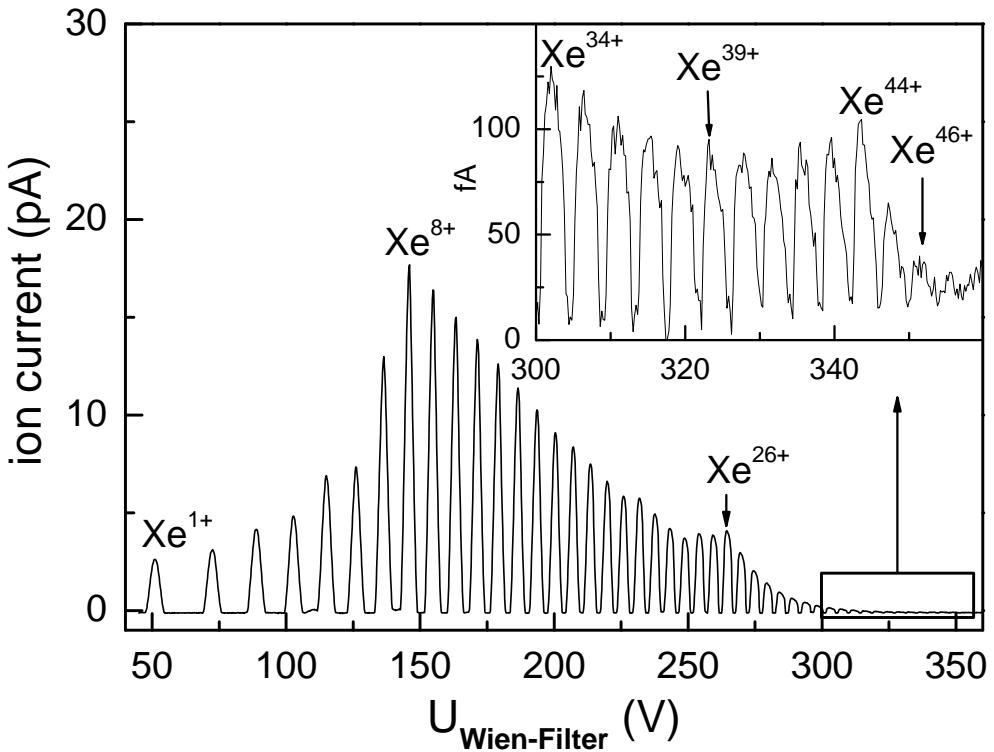


Fig. 20: A leaky mode xenon ion extraction spectrum measured at an Dresden EBIS for a vacuum of 3×10^{-9} mbar, an electron beam energy of 13.6 keV and an electron beam current of 30 mA.

4.4 Beams of Singly Charged Molecular Fragments und Clusters

In leaky mode EBIS can be used as sources for low charged ions from molecular fragments. The production of molecular fragments in an EBIS is of interest for various applications. This concerns issues such as studies on electronic transitions in molecules by spectroscopy of emitted electromagnetic radiation, protonation studies on complex molecules, as well as investigations on the interaction of molecule fragments with surfaces and on free molecules or gases in a corresponding gas jet. The use of a gas target may allow the production of neutral beams of different molecule fragments by charge exchange processes. Fig. 21 shows an ion extraction from a Dresden EBIT after injection of propane. Thereby all possible stoichiometric ratios of propane fragments were detected. More details about molecule fragmentation in EBIS can be found in [34].

Additionally, one can also produce more complex structures such as metal clusters. In Fig 22 this is shown for copper clusters as produced with a Dresden EBIT. The copper was introduced into the ion source by sputtering from a copper surface under gold ion irradiation. The capability of this technique is seen if we note that cluster with different isotope ratios can be clearly resolved such as $[({}^{63}\text{Cu})_3]^{1+}$, $[({}^{63}\text{Cu})_2({}^{65}\text{Cu}_1)]^{1+}$, $[({}^{63}\text{Cu})_1({}^{65}\text{Cu}_2)]^{1+}$ and $[({}^{65}\text{Cu})_3]^{1+}$. Without high effort cluster beam currents of up to 10^5 clusters per second were measured.

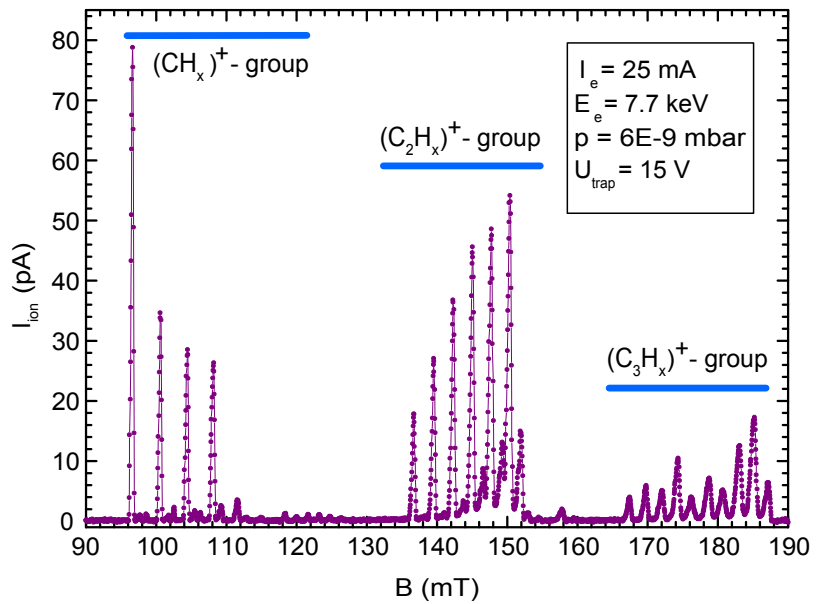


Fig. 21: Molecule fragment spectrum in leaky mode extracted from the Dresden EBIT after injection of propane.

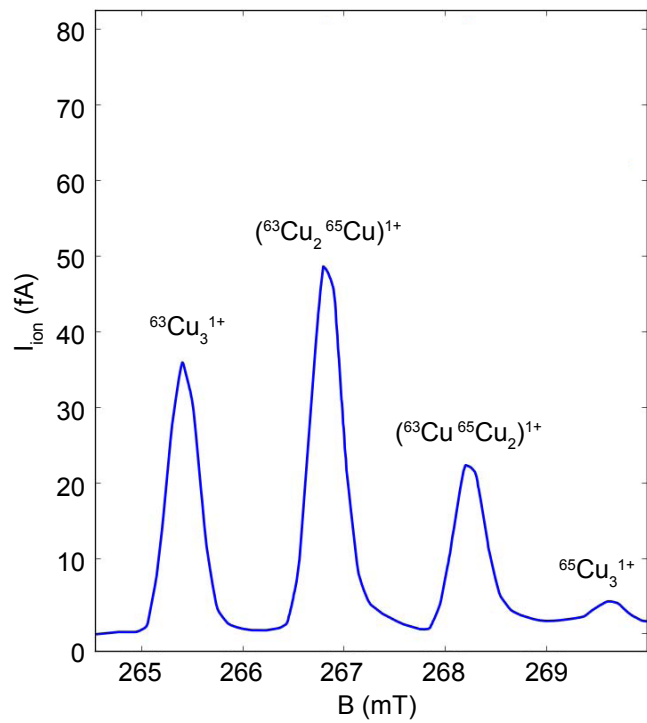


Fig. 22: Measured copper cluster from a Dresden EBIT at an electron beam energy of 6 keV and an electron beam current of 23 mA.

4.5 Absolute Numbers of Extracted Ions

To characterize the potential of different EBIS types we give some absolute ion numbers for pulsed ion extraction of ion sources of the Dresden EBIS type in Table 3. The summarized numbers characterize the expected order of magnitude for ion extraction but can deviate in dependence on the individual ion source and the selected operation regime.

Table 3: Ions per pulse for pulsed ion extraction of ion sources of the Dresden EBIS type.

Ion	Dresden EBIT	Dresden EBIS	Dresden EBIS-A	EBIT : EBIS : EBIS-A
C ⁶⁺	10.000.000	30.000.000	400.000.000	1 : 3 : 40
Ar ¹⁶⁺	900.000	8.000.000	250.000.000	1 : 9 : 280
Ar ¹⁸⁺	6.000	90.000	1.500.000	1 : 15 : 250
Xe ⁴⁴⁺	10.000	700.000	10.000.000	1 : 70 : 1000

4.6 Puls Shape for Typical Ion Extraction

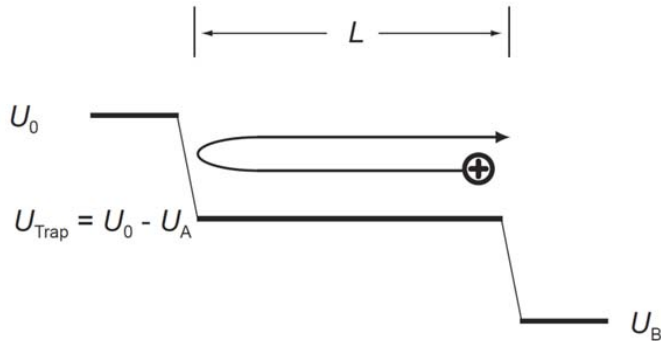


Fig. 23: Ion paths in the moment of ion extraction.

Typical puls widths at pulsed ion extraction from an EBIS are in the order of a few microseconds. Thereby the pulses are not completely symmetric but have a tail to the side of higher flight times. The reason is here that in the moment of trap opening only all ions are extracted with a flight direction towards the extraction side. All other ions will be reflected at the potential wall at the gun side and extracted after that. This situation is shown in Fig. 23. The absolute pulse width is determined by the speed of switching the trap potential at the extraction side ("slew rate"). We see that we can influence the puls width from some microseconds up to about 100 μ s, i.e. we come near to "flat-top" pulses. As example this is shown in Fig. 24 for ion pulses from an Dresden EBIS-A with a trap length L of 6 cm and different slew rates.

4.7 Short Time Ion Puls Extraction

For some applications the time structure of extracted beams of HCl is of fundamental interest. For example for applications in time of flight secondary ion mass spectroscopy (TOF-SIMS) and in some solid state physics experiments the formation of short pulses up to the ns-range is of interest. Present studies prove that a short pulsed ion extraction from the Dresden EBIT is possible. The extracted ion charges per pulse are in the range of some femtocoulombs and it is possible to extract several pulses until the trap has to be reloaded. The maximum extracted ion charge significantly depends on the chosen extraction time. As example we show in Fig. 25 a plot of extracted ion charges for Ar¹⁶⁺ pulse in dependence on the extraction time t_{extr} . From Fig. 25 it is seen that after some hundreds of ns the extracted ionic charge increase no furthermore.

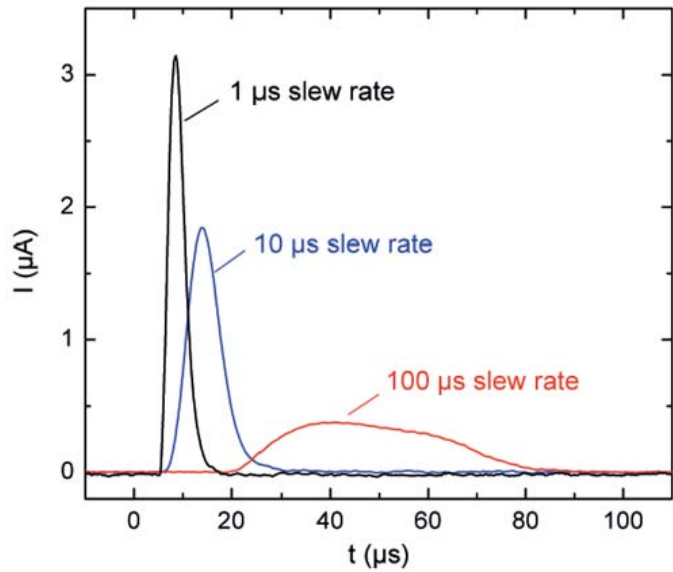


Fig. 24: Carbon ion pulses from a Dresden EBIS-A for different slew rates.

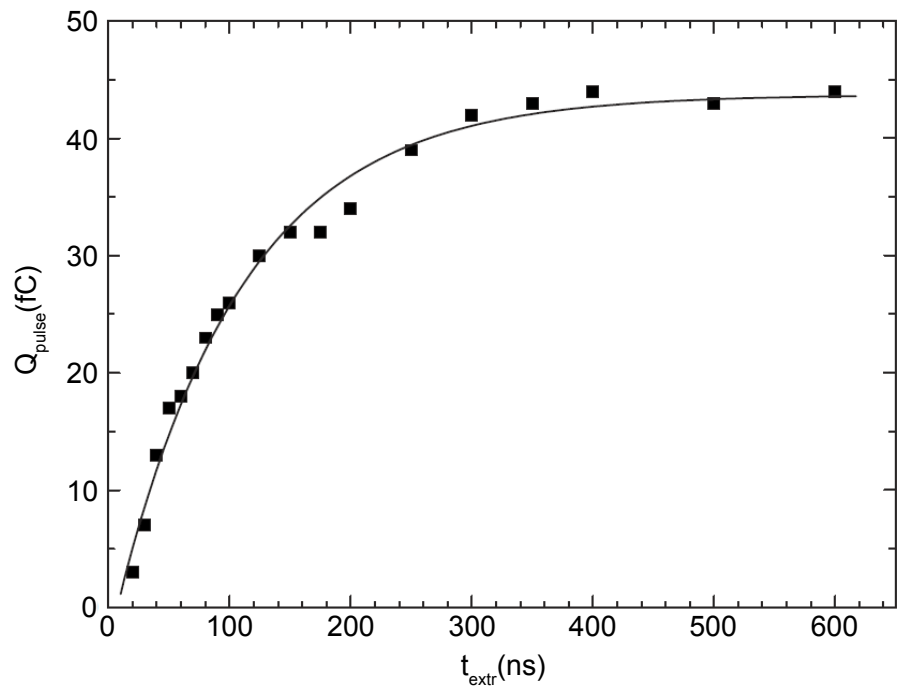


Fig. 25: Extracted ion charges of Ar^{16+} pulses from a Dresden EBIT in dependence on the extraction time t_{extr} (after [35]).

4.8 Ion Beam Emittance

For applications of ion beams a quantitative measure of the quality of the beam is given by the root-mean-square (RMS) emittance

$$\varepsilon_{x,rms} = \sqrt{\bar{x^2}\bar{x'^2} - \bar{x'}^2} \quad (34)$$

in $x - x'$ trace space and equivalent in case of $y - y'$.

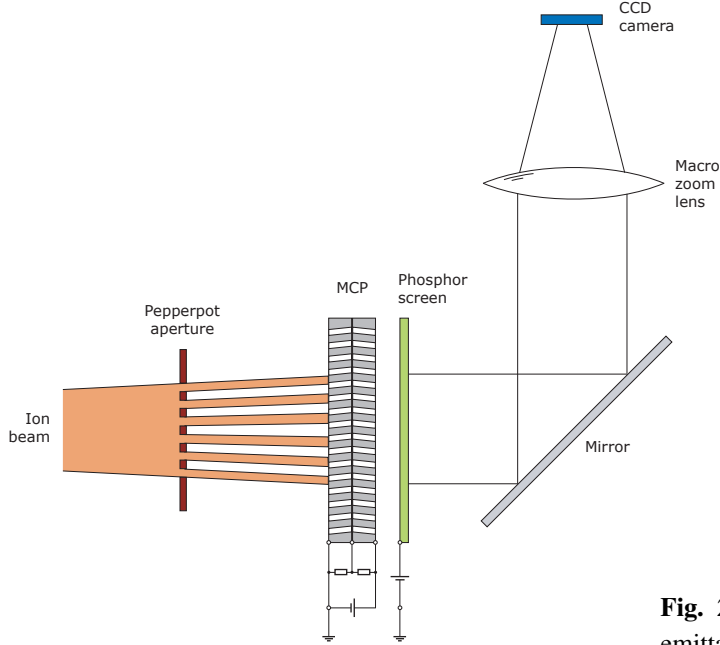


Fig. 26: Scheme of a pepperpot emittance meter.

A common method to determine these ion beam parameters is the pepper-pot technique which can be traced back to works of the 1960s [36]. A scheme of a pepperpot emittance meter is shown in Fig. 26. The incoming ion beam passes the pepperpot mask and is separated into several beam spots. The particles hitting the MCP create an electron current which is amplified passing the two micro channel plates. The electrons are then accelerated towards the phosphor screen. The visible light spots created at the phosphor screen are detected after 90° deflection by a CCD camera. The emittance of the ion beam can be determined from the positions, the sizes, and the shapes of the light spots.

Because of the small ionization volume and the small electron beam diameter EBIS produce ion beams with very low emittances. As example in Fig. 27 the x and y RMS emittance for C⁶⁺ ions extracted from a Dresden EBIS-A is shown as a function of the electron beam current. Typical emittances are in the order of some mm mrad.

For higher beam energies the pulse components perpendicular to the beam direction are small compared with the pulse components in beam direction, i.e. higher beam energies lead to lower emittances. This can be described by the normalized emittance and it yields

$$\varepsilon_{norm} = \beta' \gamma' \varepsilon \quad \text{with} \quad \beta' \frac{v}{d} \quad \text{and} \quad \gamma' = \frac{1}{\sqrt{1 - \beta^2}} \quad (35)$$

with v – ion velocity and c – speed of light. For typical operation regimes of EBIS the normalized emittance is in the order of 10⁻³ mm mrad.

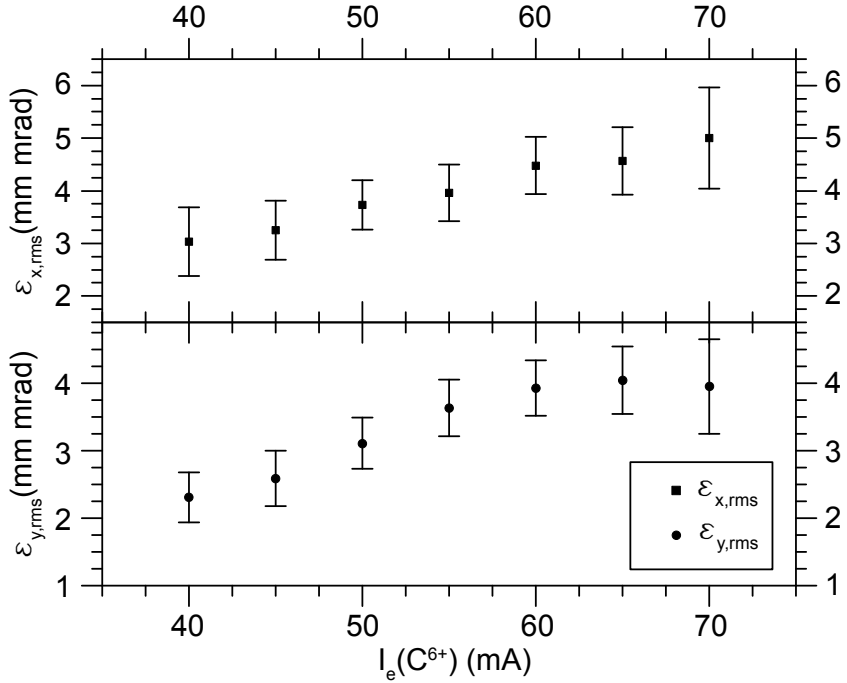


Fig. 27: RMS emittance of C^{6+} ions extracted from a Dresden EBIS-A.

4.9 Energy Spread and Absolute Energy of Extracted Ions

In order to measure the absolute energy and the energy spread of extracted ions a retarding field analyzers can be applied.

A Retarding Field Analyzer (RFA) is an electrostatic energy analyzer which allows for measuring the kinetic energy distribution of an ion beam. The analyzer consists of a collimator with exchangeable apertures, three meshes, with the central mesh set on high potential, and a Faraday cup for current measurement.

The ion or electron current is measured in the Faraday Cup of the RFA. In order to analyze the energy distribution of the incoming ion beam the potential of the retarding mesh is increased stepwise while measuring the current in the cup. The measured dependency $I_{ion}(U_{RFA})$ is differentiated and fitted with a Gaussian to obtain the energy distribution. The mean energy of the charged particles E_m is defined as the center position of the Gaussian. The energy spread of the charged particle beam ΔE is defined as the full width half maximum (FWHM) of the Gaussian.

Figures 28 and 29 show examples of measured absolute energies and energy spread of ions extracted from a Dresden EBIS-A. The energy spread of the ion beam which depends on the electron beam current is generally quite small for Dresden EBIS/T systems. For the Dresden EBIS-A it is in the order of several eV. More details about the RFA technique can be found in [37].

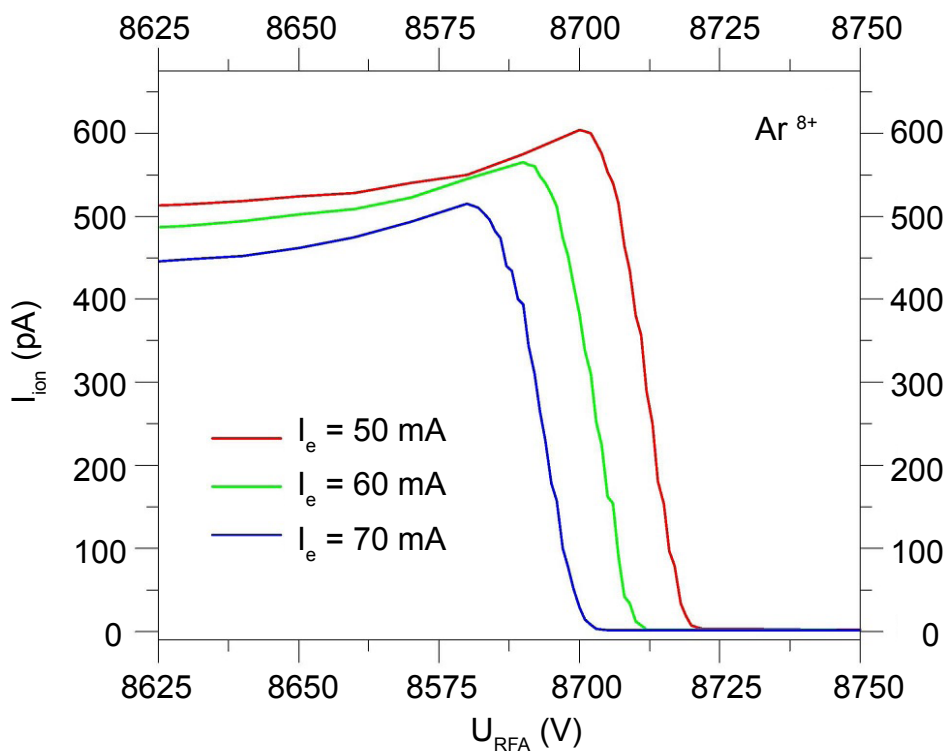


Fig. 28: $I_{\text{ion}}(U_{\text{RFA}})$ - curves for electron currents of 50, 60 and 70 mA measured with Ar^{8+} at a drift tube potential of 8.7 keV at a Dresden EBIS-A.

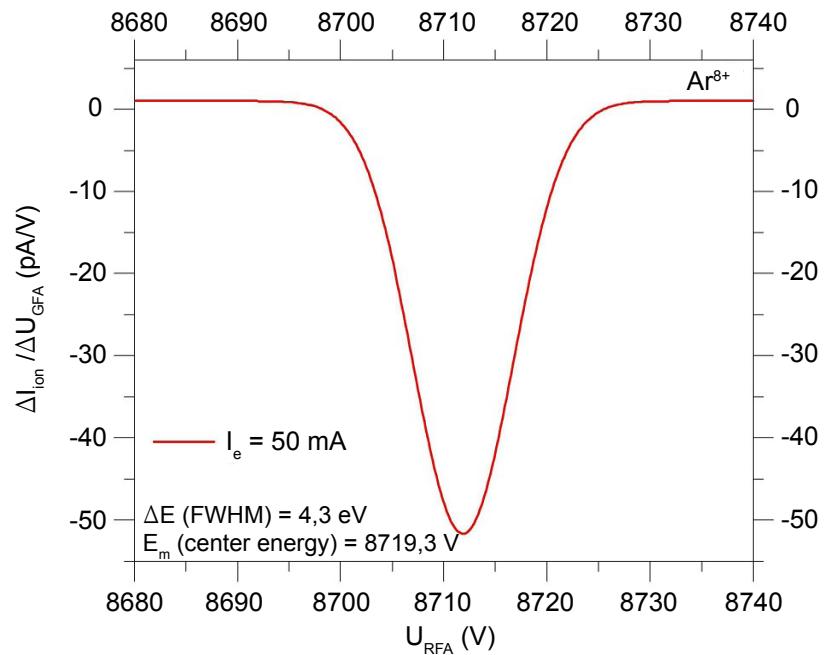


Fig. 29: The energy distribution of the extracted ion beam is $E = 4.3 \text{ eV}$ at an electron beam of $I_e = 50 \text{ mA}$ measured at a Dresden EBIS-A.

5 EBIS as Sources of X-Rays from HCIs

5.1 X-Ray Emission from HCIs

EBIS are excellent tools for x-ray spectroscopy of highly charged ions. X-rays from HCIs are of fundamental interest for atomic physics, plasma diagnostics, astrophysics and other applications. In contrast to other sources of x-rays from HCIs such as hot plasmas or accelerator facilities EBISs are comparatively small and low-cost devices. Additionally, they offer the possibility to control the electron beam energy very precisely which creates superior conditions for advanced experiments studying X-rays from HCIs.

It is well known that vacancies in the atomic shell influence X-ray lines considering their transition energies, transition probabilities and the structure of the measured spectrum. Classical X-ray spectra have been known over more than 100 years. Already in 1917 Barkla received a Nobel price for the discovery of characteristic X-rays. Less than 50 years later, in 1962, the first X-ray source outside our solar system was observed and from this date the interest in X-rays from HCIs has grown more and more.

Compared to classical X-rays as parent diagram lines appearing after the production of an inner-shell vacancy and subsequent filling of this vacancy with an outer electron, X-rays from HCIs can be different from these classical transitions. Mainly, we can observe X-ray transitions from

- Direct Excitation (DE),
- Radiative Recombination (RR) and
- Dielectronic Recombination (DE).

Detailed information on basic physics of X-rays from HCIs can be found for example in [38, 39]. Measurements were performed by different groups working with EBISs, the pioneering work of the Livermore group by Dr. Beiersdorfer et al. should be pointed out especially (see for example [40]).

5.2 X-Ray Measurements

Measurements show that in case of the Dresden EBIT individual dipole lines have a radiation power in the order of some nW. For the Dresden EBIS-A this power increases by about one order of magnitude and for the superconducting Dresden EBIS-SC by a factor of about 200. As a rule the emitted number of X-rays is high enough to perform energy dispersive as well as wavelength dispersive X-ray spectrometry in acceptable time frames of minutes up to some hours.

In Fig. 30 a measured wavelength dispersive DE spectrum from carbon- to helium-like iron ions is shown. The measurement was realized with a flat crystal and for an electron beam current of 40 mA.

Fig. 31 shows an argon RR spectrum as measured with a Dresden EBIT. Here the electron capture into the highest possible argon charge state is shown with a clear signature.

DE as well as RR measurements can be realized with comparatively simple detection techniques. In both cases without any synchronization with the EBIS a detector can measure the emitted X-rays passing through a spectroscopic window. More sophisticated are measurements of DE processes where the measurement process must be synchronized with the electron beam energy because DE processes are sharp resonance processes. For example in Fig. 32 a krypton DE KLL spectrum for Kr^{28+} up to Kr^{32+} ions is shown.

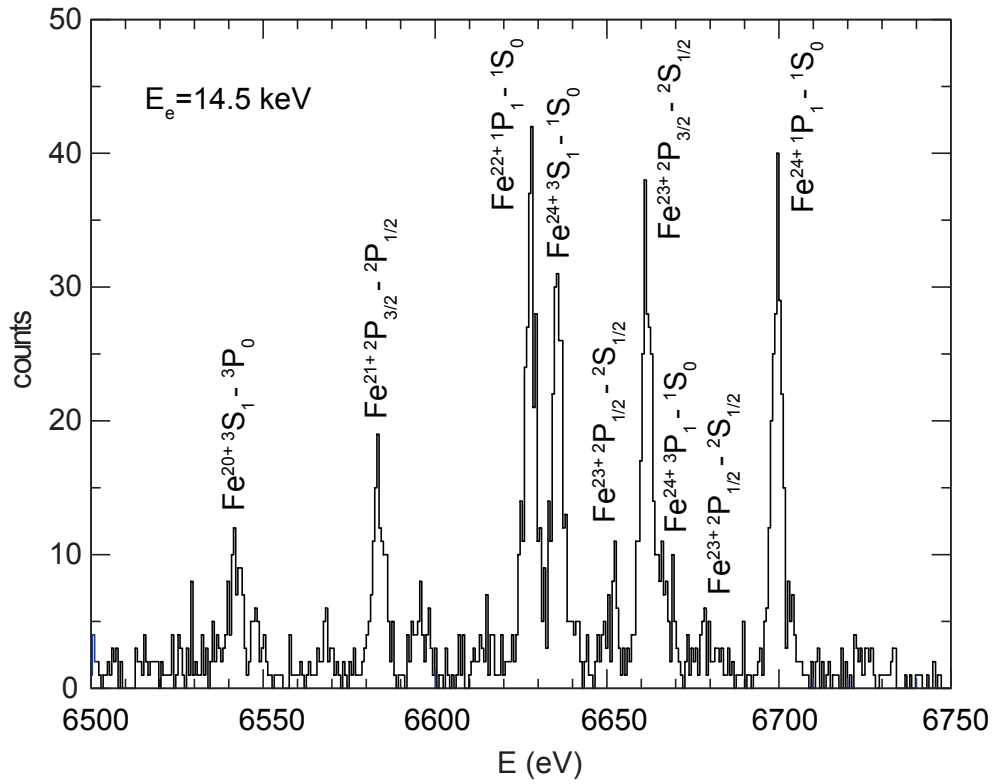


Fig. 30: Wavelength dispersive iron X-ray spectrum from DE processes in a Dresden EBIT at 14.5 keV electron beam energy.

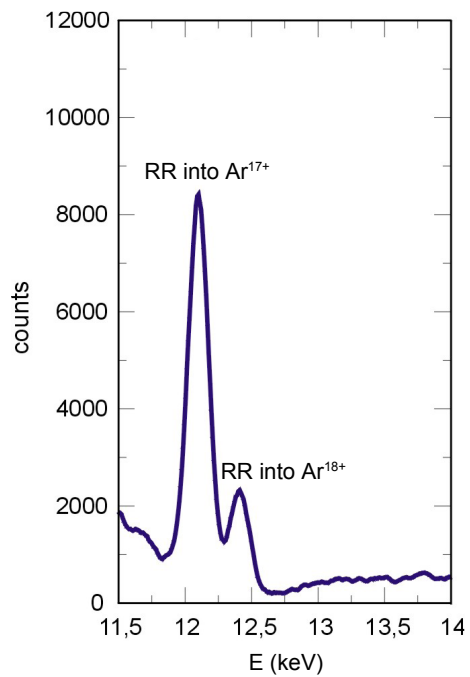


Fig. 31: Energy dispersive measured argon RR spectrum from a Dresden EBIT for the electron capture into hydrogen-like and bare argon at an electron beam energy of 8 keV and an electron beam current of 15 mA.

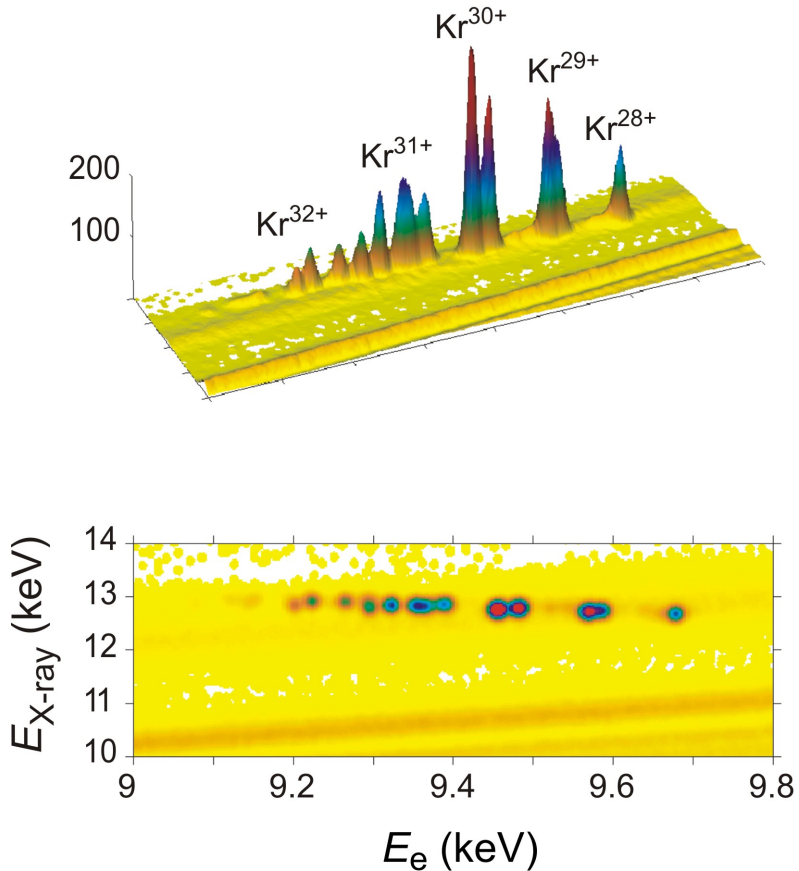


Fig. 32: Krypton KLL spectrum from DE processes for Kr^{28+} up to Kr^{32+} ions in a Dresden EBIT.

Additionally to the classical energy or wavelength dispersive X-ray spectroscopy time-resolved X-ray spectrometry is possible if we add to each measured count a time information about the ionization time in the ion trap (time between closing the ion trap and registration of the X-ray quanta). Such a spectrum is shown in Fig. 33 for a Kr^{28+} DE KLL X-ray transition. The Figure shows the evolution of the Kr^{28+} ionization charge state in the ion trap of a Dresden EBIT and demonstrates that such ions can be stored for 10 s or longer.

6 Applications of EBIS (Selected Topics)

As mentioned at the beginning, EBIS are versatile tools for investigations on HCIs in basic and applied research as well as for applications with strong practical relevance. It is not the aim of the present paper to discuss all these topics in detail, but in the following subsections we will give some examples on the versatile application potential of HCIs.

6.1 HCI-FIB for Structuring and Surface Analysis

Standard Focused Ion Beam (FIB) systems use Liquid Metal Ion Sources (LMIS) with their rather small standard spectrum of projectiles. Combining an EBIS which provides a broader palette of ion species from different elements (from noble gases up to metals) ranging from high to low charge states with a FIB column leads to new usable physical properties and new applications.

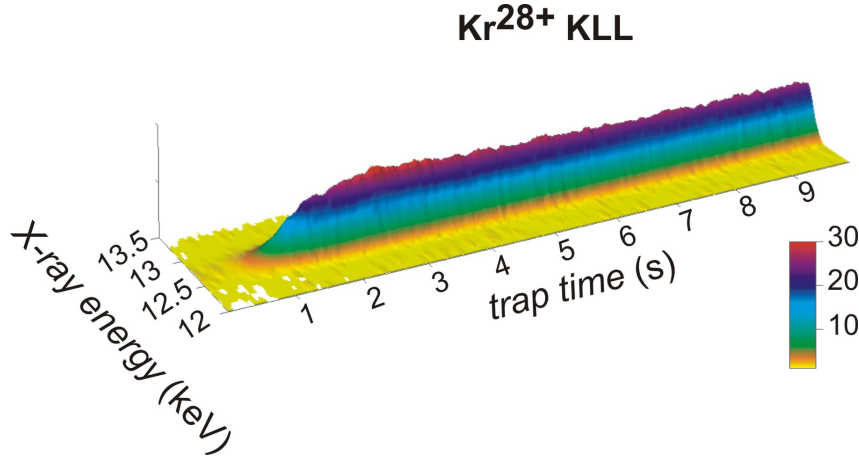


Fig. 33: Time-resolved krypton DE KLL spectrum for Kr^{28+} measured at a Dresden EBIT.

As already introduced, the potential energy stored in the highly charged ions due to the ionization process leads to power densities of 10^{12} up to 10^{14} W/cm^2 in single ion-surface interactions and therefore to higher yields of secondary ions and secondary electrons per incident ion compared to conventional ions. Preliminary experiments have been done at the CNRS in Marcoussis ([41]).

Furthermore, the ion implantation range can be varied by selecting a certain charge state which is due to the final kinetic energy at a constant acceleration potential (see Figure 34). This can be realized via the integration of a crossed-field ion beam separator, the already introduced Wien filter ([33]), which enables the user to separate the ions according to their mass-to-charge ratio. Since the ion energy depends on the charge state as well as on the mass a broad range of projectile energies is available. Also, the intrinsic potential energy of the projectile can be adjusted by the user by selecting the charge state of the ions.

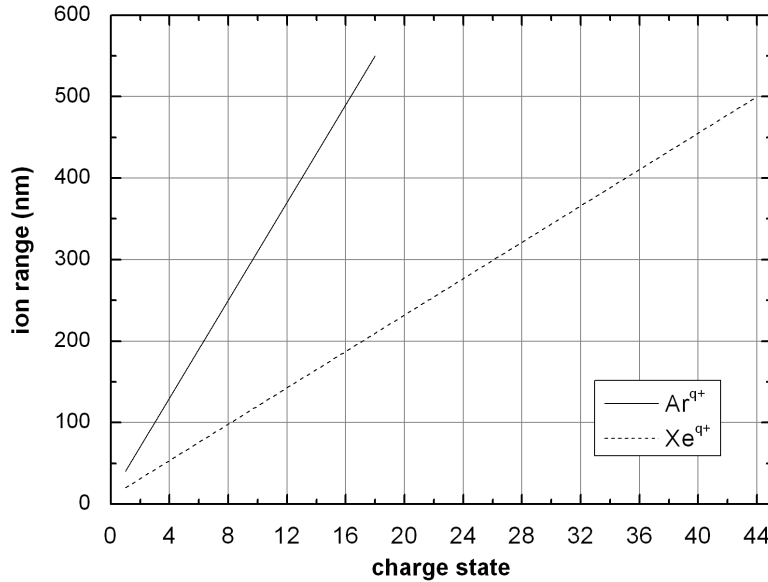


Fig. 34: Ion range of argon and xenon ions in silicon at different kinetic energies.

The technology as described above complements the classical spectrum of projectiles for various applications beyond the latest developments using noble gas ions in FIB systems. Considering the ion charge state as a new physical parameter which can be varied offers suitable preconditions in sputtering processes in regard to the produced secondary particles being used for surface analysis (Time Of Flight - Secondary Mass Spectroscopy). This also considers the ability to vary the kinetic energy at a fixed acceleration potential of the ion source and FIB column assembly.

6.2 Particle Therapy

Cancer is the second most common cause of death worldwide and, statistically, about 33% of all inhabitants of the European Union will be confronted with some kind of cancer in their lives. Currently about 45% of all cancer cases can be treated, mainly by surgery and/or by radiation therapy [42].

Within the radiotherapy, the radiation with hadrons (mainly protons and carbon ions) is the most promising treatment technique. In contrast to the classical irradiation with X-rays the treatment with ions has significant advantages. The energy deposition within the tissue obey to the Bragg interaction. I.e. the maximum of the energy is deposited at the end of the particle trajectories, hence in the tumour cells. The ion range can be adjusted precisely by varying the kinetic energy of the particles. Intruding ions loose energy inside a dense medium according to the bragg curve. Most of the kinetic energy is deposited in a certain depth along the ion path. This effect can be used to destroy a tumor while the healthy tissue around is spared (important for tumours in the vicinity of risky organs like the medulla).

Another important property of ions as opposed to photons is their electrical charge. Charged particles can be focused and deflected by electrical and magnetic fields, providing the ability to scan with the ion beam over the tumour very precisely. Due to the variation of the kinetic energy of the ions it is possible to vary the penetration depth. Hence the tumour can be scanned voxel by voxel (a voxel is a three dimensional volume element). Besides the electrical properties the relative biological efficiency (RBE) of the ions is higher by a factor of about three. This means that the same dose of carbon ions effects the tumour tissue by a factor of 3 more compared to classical x-rays. The higher RBE allows a lower dose by the same effect on the tumour with less damage of the healthy tissue.

Nowadays, a substantial number of medical particle therapy facilities are based on synchrotron accelerators combined with ECR ion sources. Due to the low purity of the ion beam electron strippers are required. If using an EBIS ion source and its excellent beam purity a subsequent electron stripper is not necessary anymore. Also, the lower emittance of EBIS sources will lead to a higher transparency of the accelerator structure. For other accelerator strategies like direct wall accelerators or direct driven accelerators even the application of room temperature EBIS ion sources might be possible.

6.3 Charge Breeding

In nuclear mass measurements involving ions stored in Penning traps the precision of the experimental method increases proportionally with the charge state of the investigated ions. Furthermore, for proposed nuclear fusion reaction studies neutron-rich, relatively short-lived radioactive isotopes have to be accelerated to energies above the Coulomb barrier, which requires a small mass to charge ratio (A/q) to reduce the scale and cost of the accelerator. These and other endeavours rely on the availability of HCI from a broad spectrum of elements or even exotic radioactive species, respectively.

As described above, EBIS or EBIT are HCI sources which have many advantages, however, they are typically loaded via gas injection which limits the range of available ion species from these machines. The injection of externally produced low charged ions into an EBIS or EBIT and re-extraction as HCIs, known as charge breeding, offers a way to increase the range of available HCI species. Various ion injection techniques have been used for charge breeding. Among these are experimental setups including Metal Vapor Vacuum Arc and Liquid Metal or Liquid Metal Ion Sources [43, 44] but also beams of short lived radioactive isotopes produced using the ISOL technique [46].

Recently, a Dresden EBIS-A was fed by a Liquid Metal Alloy Ion Source to produce HCI from low charged gold ions. For the charge bred Au^{q+} ions charge states up to $q = 60$ were achieved (see Figure 35). This experimental technique represents a clean and elegant way of introducing metals or other elements into the Dresden EBIS-A which cannot be injected directly through a gas valve. Therefore, the range of applications for this type of ion source is extended.

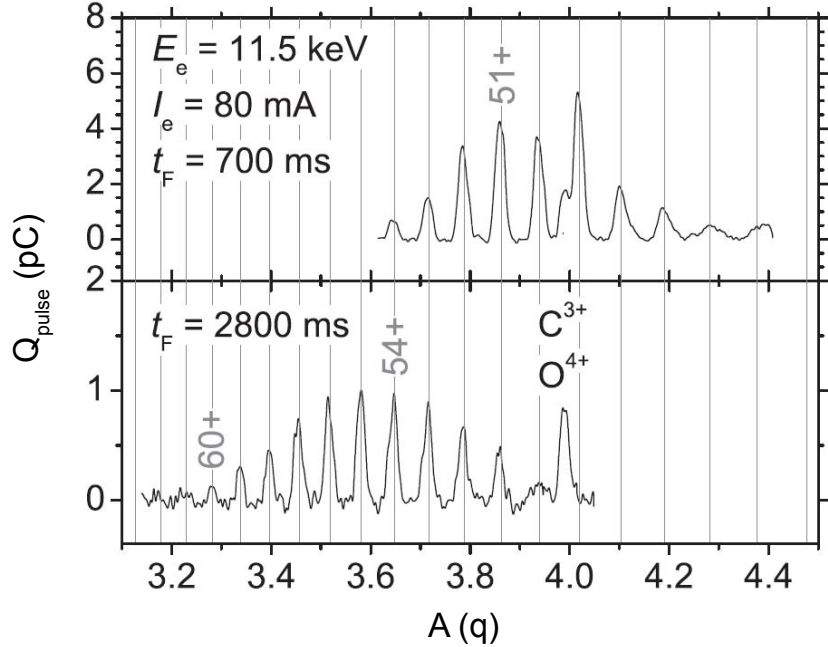


Fig. 35: Charge breeding spectra with gold ions injected into the trap of an EBIS-A with an external LMIS (from [45]).

7 Conclusion

Highly charged ions (HCIs) become more and more important in basic research as well as technological applications. This is because of their unique properties which are listed shortly in the beginning of this text. In the past, large accelerator devices had to be used for the production of HCIs while todays sources of HCIs fit on the top of a table. This increases the availability of HCIs and opens up new possibilities for a larger community to realize experiments with HCIs.

This paper highlights the electron beam ion source (EBIS) technology as an efficient and elegant way to produce HCIs. The basic physics and working principle of EBIS are explained in detail and compared to other existing HCI sources. Especially, aspects of HCI extraction but also the use of EBISs as sources of X-rays from HCIs trapped inside the machines are discussed.

Hopefully this work inspires researchers to continue the advancement of this extraordinary ion source technology and creates ideas for new fields of applications of HCIs produced by EBISs in the future.

References

- [1] I.S.Bowen, R.A.Millikan, Physical Review, 25 (1925) 591
- [2] B.Edlen, Z.Astrophys., 22 (1942) 30
- [3] R.Geller, *Electron Cyclotron Resonance Ion Sources and ECR Plasmas*, IOP Publishing, Bristol 1996
- [4] B.Sharkov, *Laser Ion Sources*, in *The Physics and Technology of ion Sources*, 2nd ed., Wiley-VCH, Berlin 2004
- [5] J.Gillaspy, *Trapping Highly Charged Ions: Fundamentals and Applications*, Nova Science Publishers Inc., Huntington, New York 2001
- [6] F.Currell, *Electron Beam Ion Traps and their Use in the Study of Highly Charged Ions*, in: *The Physics of Multiply and Highly Charged Ions*, Vol. I, ed. by F.Currell, Kluwer Academic Publishers, Dordrecht-Boston-London 2003
- [7] J.Gillaspy, Journal of Physics B: Atomic, Molecular and Optical Physics, 34 (2001) R93
- [8] H.F.Beyer, V.P.Shevko, *Introduction to the Physics of Highly Charged Ions*, IOP Bristol and Philadelphia 2003
- [9] E.D.Donets, USSR Inventor's Certificate No. 248860 16.03. (1967); Bull. OIPOTZ 24 (1969) 65
- [10] E.D.Donets, V.I.Ilushenko, V.A.alpert, *Ultrahigh vacuum electron beam ion source of highly stripped ions*, in: *Proceedings of the First International Conference on Ion Sources*, Saclay (France), 1969, p.635
- [11] E.D.Donets, V.P.Ovsyannikov, Sov.Phys. – JETP, 53 (1981) 466
- [12] M.A.Levine, R.E.Marrs, J.R.Henderson, D.A.Knapp, M.B.Schneider, Physica Scripta, T22 (1981) 157
- [13] J.W.McDonald, D.H.G.Schneider, Nuclear Instruments and Methods on Physics Research, B 241 (2005) 870
- [14] V.P.Ovsyannikov, G.Zschornack, Review of Scientific Instruments, 70 81999) 2646
- [15] see: <http://www.dreebit.com>
- [16] G.Zschornack, V.P.Ovsyannikov, F.Grossmann, A.Schwan, F.Ullmann, Proceedings of the International Symposium on Electron Beam Ion Sources and Traps, April 7-10 2010, Stockholm (Sweden), JINST 5 C08012
- [17] R.Becker, O.Kester, Review of Scientific Instruments, 81 (2010) 02A513
- [18] J.W.Mcdonald, D.H.G.Schneider, Nuclear Instruments and Methods in Physics Research, B 241 (2005) 870
- [19] V.P.Ovsyannikov, Doctor Thesis "*Technique and Application of Electron Beam Ion Sources*", Joint Institute of Nuclear research, Dubna, Russia, 1996
- [20] W.Lotz et al., Z.Phys., 206 (1967) 205
- [21] T.Werner, Diploma Thesis, Institut fuer Kern- und Teilchenphyik, TU Dresden, Dresden, 1997
- [22] A.Mueller, R.Frodel, Physical Review 44 (1980) 29
- [23] A.Mueller, E.Salzborn, Phys.Lett. A59 (1976) 19
- [24] F.Ullmann, PD Thesis, Technische Universitaet Dresden, Fakultaet Mathematik und Naturwissenschaften, Dresden, 2005
- [25] Y.S.Kim, R.H.Pratt, Physical Review A27 (1983) 2913
- [26] R.Becker, Talk on ICIS 2009, Gatlinburg, USA
- [27] B.M.Penetrante, J.N.Bardsley, D.DeWitt, M.Clark, D.Schneider, Physical Review A43 (1991) 4861
- [28] I.V.Kalagin, D.Kuechler, V.P.Ovsyannikov, G.Zschornack, Plasma Sources Sci. Technol. 7 (1998) 441
- [29] G.Herrmann, J.Appl.Phys., 29 (1958) 127

- [30] H.Kuramoto, T.Kinnugawa, H.Watanabe, C.Yamada, S.Ohtani, I.Yamada, F.J.Currell, Rev.Sci.Instrum. 73 (2002) 42
- [31] A.Thorn, PhD Thesis, Technische Universitaet Dresden, Fakultaet fuer Mathematik und Naturwissenschaften, Dresden, 2012
- [32] G.Zschornack, A.Schwan, F.Ullmann, F.Grossmann, V.P.Ovsyannikov, E.Ritter, Review of Scientific Instruments 83 (2012) 02A507
- [33] M.Schmidt, H.Peng, G.Zschornack, S.Sykora, Review of Scientific Instruments 80 (2009) 063301
- [34] M.Kreller, G.Zschornack, U.Kentsch, R.Heller, Review of Scientific Instruments 79 (2008) 02A702
- [35] U.Kentsch, G.Zschornack, A.Schwan, F.Ullmann, Review of Scientific Instruments 81 (2010) 02A507
- [36] L.E.Collins, P.T.Stroud, Nuclear Instruments and Methods 26 (1964) 157
- [37] E.Ritter, Diploma Thesis, Technische Universitaet Dresden, Department of Physics, Dresden, 2010
- [38] H.F.Beyer, H.-J. Kluge, V.P.Shevko, *X-Ray Radiation of Highly Charged Ions*, Springer, Berlin and Heidelberg, 1997
- [39] *The Physics of Multiply and Highly Charged Ions*, Vol. 1, ed. by F.J. Currell, Kluwer Academic Publishers, Dordrecht, Boston and london, 2003
- [40] P.Beiersdorfer, AIP Conference Proceedings 389 (1997) 121
- [41] F.Ullmann, F.Grossmann, V.P.Ovsyannikov, J.Gierak, G.Zschornack, Appl. Phys. Lett. 90 (2007) 083112
- [42] S.Peggs, PAC07, June 25th, 2007
- [43] N.Nakamura, T.Kinugawa, H.Shimizu, H.Watanabe, S.Ito, S.Ohtani, C.Yamada, K.Okazaki, M.Sakurai, M.R.Tarbutt, J.D. Silver, Rev. Sci. Instr. 71 (2000) 684
- [44] A.Pikin, J. G. Alessi, E. N. Beebe, A. Kponou, and K. Prelec, Rev. Sci. Instrum. 77 (2006) 03A909
- [45] A. Thorn, E. Ritter, F. Ullmann, W. Pilz, L. Bischoff, G. Zschornack, Rev. Sci. Intrum. 83 (2012) 02A511
- [46] F. Wenander, J. Instrum. 5 (2010) C10004
- [47] R.W.Schmieder, R.J.Bastasz, VIth International Conference on the Physics of Highly Charged Ions, AIP Conference Proceedings 274, Manhattan, KS 1992
- [48] G.Zschornack, F.Grossmann, V.P.Ovsyannikov, R.Heller, U.Kentsch, M.Kreller, M.Schmidt, A.Schwan, A.Silze, F.Ullmann, Materialwissenschaften u. Werkstofftechnik 40 (2009) No. 4, 1
- [49] V.Shevko, H.Tawara (editors), *Atomic Processes in Basic and Applied Physics*, Springer Heidelberg, New York, Dordrecht and London, 2012